AD-A218 433

AD

US ARMY
LABORATORY COMMAND
MATERIALS TECHNOLOGY LABORATORY

MTL TR 89-96

REAL-TIME STEREO-MICRORADIOGRAPHY

November 1989

D. POLANSKY, R. PLACIOUS, E. CRISCUOLO,
E. GAYNOR, and H. BERGER
Industrial Quality, Inc.
19634 Club House Road
Gaithersburg, MD 20879

FINAL REPORT   Contract DAAL04-87-C-0074

Prepared for

U.S. ARMY MATERIALS TECHNOLOGY LABORATORY
Watertown, Massachusetts 02172-0001

90 02 23 039

REPORT DOCUMENTATION PAGE	READ INSTRUCTIONS BEFORE COMPLETING FORM

1. REPORT NUMBER MTL TR 89-96	2. GOVT ACCESSION NO.	3. RECIPIENT'S CATALOG NUMBER

4. TITLE (and Subtitle) REAL-TIME STEREO-MICRORADIOGRAPHY	5. TYPE OF REPORT & PERIOD COVERED Final Report 9/87 to 9/89
	6. PERFORMING ORG. REPORT NUMBER IQI-DFR-89-1006

7. AUTHOR(s) D. Polansky, R. Placious, E. Criscuolo, E. Gaynor, H. Berger, J. Reed,* R. Schirato,* R. Polichar,* and J. Baltgalvis*	8. CONTRACT OR GRANT NUMBER(s) DAAL04-87-C-0074

9. PERFORMING ORGANIZATION NAME AND ADDRESS Industrial Quality, Inc. 19634 Club House Road Gaithersburg, MD 20879	10. PROGRAM ELEMENT, PROJECT, TASK AREA & WORK UNIT NUMBERS

11. CONTROLLING OFFICE NAME AND ADDRESS U.S. Army Materials Technology Laboratory ATTN: SLCMT-PR Watertown, MA 02172-0001	12. REPORT DATE November 1989
	13. NUMBER OF PAGES 84

14. MONITORING AGENCY NAME & ADDRESS(if different from Controlling Office)	15. SECURITY CLASS. (of this report) Unclassified
	15a. DECLASSIFICATION/DOWNGRADING SCHEDULE

16. DISTRIBUTION STATEMENT (of this Report)

Approved for public release; distribution unlimited.

17. DISTRIBUTION STATEMENT (of the abstract entered in Block 20, if different from Report)

18. SUPPLEMENTARY NOTES

*Science Applications International Corporation, 10401 Roselle Street, San Diego, CA 92121

COR: J. Antal, Materials Testing & Evaluation Branch, MTL

19. KEY WORDS (Continue on reverse side if necessary and identify by block number)

X-ray inspection	Depth measurement	Composite materials
Real-time X-ray imaging	Nondestructive testing	
Stereo imaging	Ceramics	

20. ABSTRACT (Continue on reverse side if necessary and identify by block number)

(SEE REVERSE SIDE)

Block No. 20

ABSTRACT

A new real-time stereo X-ray imaging system is described. Fast X-ray source movement (TV field of 1/60 s) is possible in a microfocus X-ray source by electromagnetic shifting of the electron beam. The two-view fields are combined in a TV frame for stereo viewing through a polarizing screen. Real-time, stereo X-ray images of moving inspection objects can be followed. One can view the stereo X-ray images to judge the apparent depth of an X-ray indication. One can also measure the depth of selected indications with a developed software system. This report describes the development of this novel stereo X-ray inspection system over the two-year period of this SBIR, Phase II project. Plans are being made to offer the stereo, depth measurement system commercially.

SUMMARY

The objective of this Small Business Innovation Research (SBIR) program was to develop a prompt-response, X-ray-imaging system for the nondestructive inspection of ceramics, composites, and other materials and assemblies. The television-displayed X-ray image can be viewed by the inspector to gain an impression of detail depth within the inspection object. In addition, a software method to mark one or more details and measure their depths has been demonstrated. The use of a microfocus X-ray source offers advantages for this application. One, the geometric magnification and improved X-ray-image spatial resolution available (to values in the order of 10 to 20 line pairs/mm) makes the inspection system particularly useful for the inspection of ceramics--an application in which the detection of small discontinuities (.05 mm or less) is vital. Secondly, the microfocus X-ray source used at geometric magnifications of 10 to 20x lends itself well to small movements of the X-ray source electron beam to generate useful stereo views. This small movement (a few mm) can readily be accomplished within the X-ray tube using either internal or external magnetic deflection.

The development has shown that the dual X-ray views for depth measurement can be accomplished either by the electron-beam movement within the microfocus X-ray source or by the physical movement of the X-ray source. Useful depth-measurement methods have been demonstrated for both approaches.

Accession For		
NTIS GRA&I	☑	
DTIC TAB	☐	
Unannounced	☐	
Justification		
By		
Distribution/		
Availability Codes		
Dist	Avail and/or Special	
A-1		

FOREWORD

This document reports the results of a two-year Small Business Innovation Research (SBIR) investigation directed toward the development of a real-time stereo-microradiographic system. This prompt-response, electronic X-ray imaging system offers particular advantages for X-ray inspection of ceramics, composites, castings, welds, and electromechanical assemblies. The work was funded by the Army Materials Technology Laboratory under contract DAAL04-87-C-0074. The development involves the movement of the imaging X-ray source, either electronically or physically, to generate different X-ray views of the inspection object. The different views are presented as television fields for stereo viewing. The combined television frame then shows the stereo image; a viewer wearing electro-optic shutter glasses synchronized to the video frame rate sees one set of fields with one eye, and the other set of fields with the other eye. The viewer thus observes the prompt-response stereo X-ray image. In addition, the depth of an X-ray detail can be measured.

TABLE OF CONTENTS

LIST OF FIGURES

1.0 INTRODUCTION

The normal X-ray inspection methods employed with film or non-film recording/imaging media present a through-transmission view of the inspected object. This reveals variations in object thickness, density, and discontinuities within the specimen. While defect detection and relative size, as projected on the x-y plane (the plane of the radiographic film or detector face) are determined, a full discontinuity characterization is not obtained. This requires the three-dimensional location of the discontinuity and the extent of the flaw in the "Z" direction (perpendicular to the plane of the projected image). This additional information, over that from the conventional image, would supply engineering-type data that would greatly aid accept/repair/reject decisions. This report describes a project whose purpose was to develop a "stereo" X-ray imaging system that has the capability of providing high-resolution conventional discontinuity characterization with the additional information about three-dimensional flaw size and its location in the object.

Conventional radiography is resolution-limited by radiographic unsharpness. One major contributor to this is X-ray source size. Microfocus systems feature source sizes two to three orders of magnitude smaller than conventional sources. This allows direct X-ray geometric magnifications of 10 to 20x, while still yielding images with low values of unsharpness. In effect, microfocus sources combined with X-ray magnification overcome resolution limits imposed by conventional systems. This project utilized microfocus sources to this end.

Other benefits derive from this new approach. First, discrete detectors and image intensifiers can be used even though their inherent resolution (line pairs per unit length) is inferior to that of film. Magnification obviates the need for very-high-resolution-detecting media. Secondly, microfocus sources produce a very large depth of field in the image. The discontinuities retain image sharpness throughout the depth of the object. A third benefit results because a small displacement of the electron beam on the target translates into an effectively large displacement on the image plane as a result of the X-ray magnification. The combination of the effective large-beam displacement with the large depth of field

1

from the microfocus source is exactly the prescription needed for stereo X-ray imaging. The use of microfocus sources with magnification is often called microradiography, although, when discrete detectors, conventional image amplifiers, or other electronic detectors are used, the more correct designation is microradioscopy. When beam displacement is added and provisions are made for the proper display of alternating fields produced by each beam position, the designation stereo- microradiography or stereo-microradioscopy* applies.

In addition to the stereo capability, the objectives of the project included real-time electronic imaging and a capability to detect extremely small sizes of discontinuities (several micrometers), which are important in the inspection of brittle materials. The total project, therefore, involved the development of a stereo, real-time, microfocus X-ray imaging system. This system is especially well-suited to the inspection of ceramics, brittle materials in which critical defect sizes are often in the range of 10 to 100 μm. The proposed X-ray inspection system not only will detect discontinuities in the 100 μm and smaller size range, but also will provide excellent characterization capability for the detected discontinuity by virtue of the stereo imaging feature.

Indeed, almost all radiological inspections could benefit from the integration of microfocus-magnification radiography, state-of-the-art non-film (real-time) detectors, and high-quality computer-based video-imaging systems. Welds in steel or other metals, as in pipelines, for example, also have been suggested for stereo-imaging. A large part of the accept/reject criteria for pipeline flaws is governed by fracture mechanics or workmanship standards which require depth information for analysis. A third application is for composite inspection, which is one of the new materials now being extensively exploited as a metal substitute in many fabrications. It should be possible to identify three-dimensional flaw locations in composites more readily with stereo-imaging than with conventional two-dimensional radiography.

---

*Throughout this report, we will continue to use the phrase "Real-Time Stereo Microradiography" with the understanding that this project was designed and demonstrated with active (non-film) detector systems. The use of film as a detector is not excluded, except that a conventional stereo-viewer is required.

In this report, basic principles of stereo radiography will be discussed first. Then, the design considerations and fabrication of a stereo-microradiography system are discussed. Following that, system performance and other results will be presented. Included in that section is a discussion of quantitative depth-measurement techniques and results. A series of applications of the technology to various samples of interest is presented next. Sections on prospects for commercialization of stereo-microradiography and conclusions follow. A list of recommended features of a real-time stereo-radioscopic system is included as an appendix.
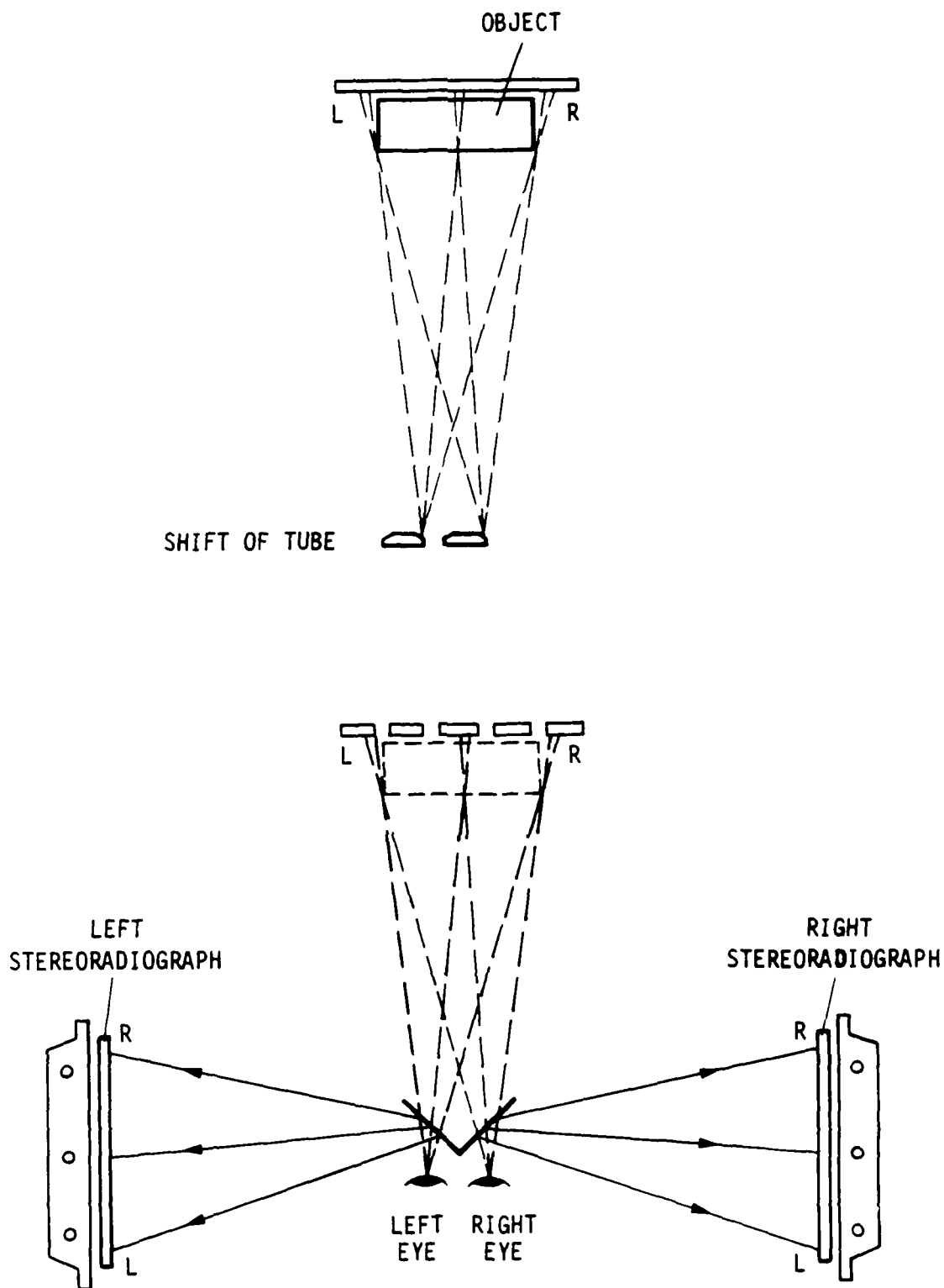
2.0   PRINCIPLES OF REAL-TIME STEREO-MICRORADIOGRAPHY

2.1   STEREOSCOPIC VIEWING

The use of stereo viewing in film-based X-radiography is not new.[1-8]   In this approach, two radiographic views of the object are made, usually by moving the X-ray source or object between views. Viewing is usually arranged with mirrors so that one eye sees only one view, while the other eye sees only the other. A typical arrangement for the radiographic shift and the viewing by each eye is shown in Figure 2-1.   Normal vision with two eyes is, by nature, stereoscopic.   The perception of depth is possible because two images of the same scene from a slightly different vantage point are simultaneously and effectively superimposed by the brain. The brain immediately combines the views received by each eye into a single mental image, giving the impression of depth and shape. In stereo-radiography, similar principles are utilized. To do this, a proper radiographic view is made for each eye. The pair of radiographic views gives the illusion of depth in the object when viewed as shown in Figure 2-1. Conventional stereo-radiography has been handicapped by the need for significant manual displacement of the X-ray source and the limited depth of field in the image. These handicaps have been overcome by the rapid development of microfocus X-ray systems and their ability to permit X-ray magnification. When on-line stereo presentation is added to this by using non-film detector systems, dynamic real-time inspection in stereo becomes feasible.

When a pair of X-ray images are taken from different angular perspectives and displayed on the TV screen as two different television fields, the viewer sees a double image since parts of the image move with respect to the other for the different views.[9,10]   However, a viewer wearing electro-optic shutter glasses synchronized to the video frame rate has a restricted view in that the right eye sees only one view and the left eye sees the other. These two alternating fields are usually called the "right" field and the "left" field, or the even-odd fields. Figure 2-2 shows the geometry of the viewing system. The symbols given in Figure 2-2 are as follows:

L = position of left eye
R = position of right eye

OBJECT

L　　　　R

SHIFT OF TUBE

L　　　　R

LEFT
STEREORADIOGRAPH

RIGHT
STEREORADIOGRAPH

R　　　　　　　　　　　　　　　　　　　R

L　　　　　　　　　　　　　　　　　　　L

LEFT　RIGHT
EYE　EYE

SAIC-89JR-70

Figure 2-1. Arrangements for Preparing and viewing Stereo-
radiographs (Adapted from McMaster, Ref. 2).

5

APPARENT
DEPTH,
OBJECT 2

3   2 1   LEFT
             EYE
             IMAGE

1   3   2   RIGHT
                          EYE
                          IMAGE

I

R1   3   L1   R2
              L2   TV SCREEN

D_A

d

APPARENT
DEPTH,
OBJECT 1

L   R

S_V
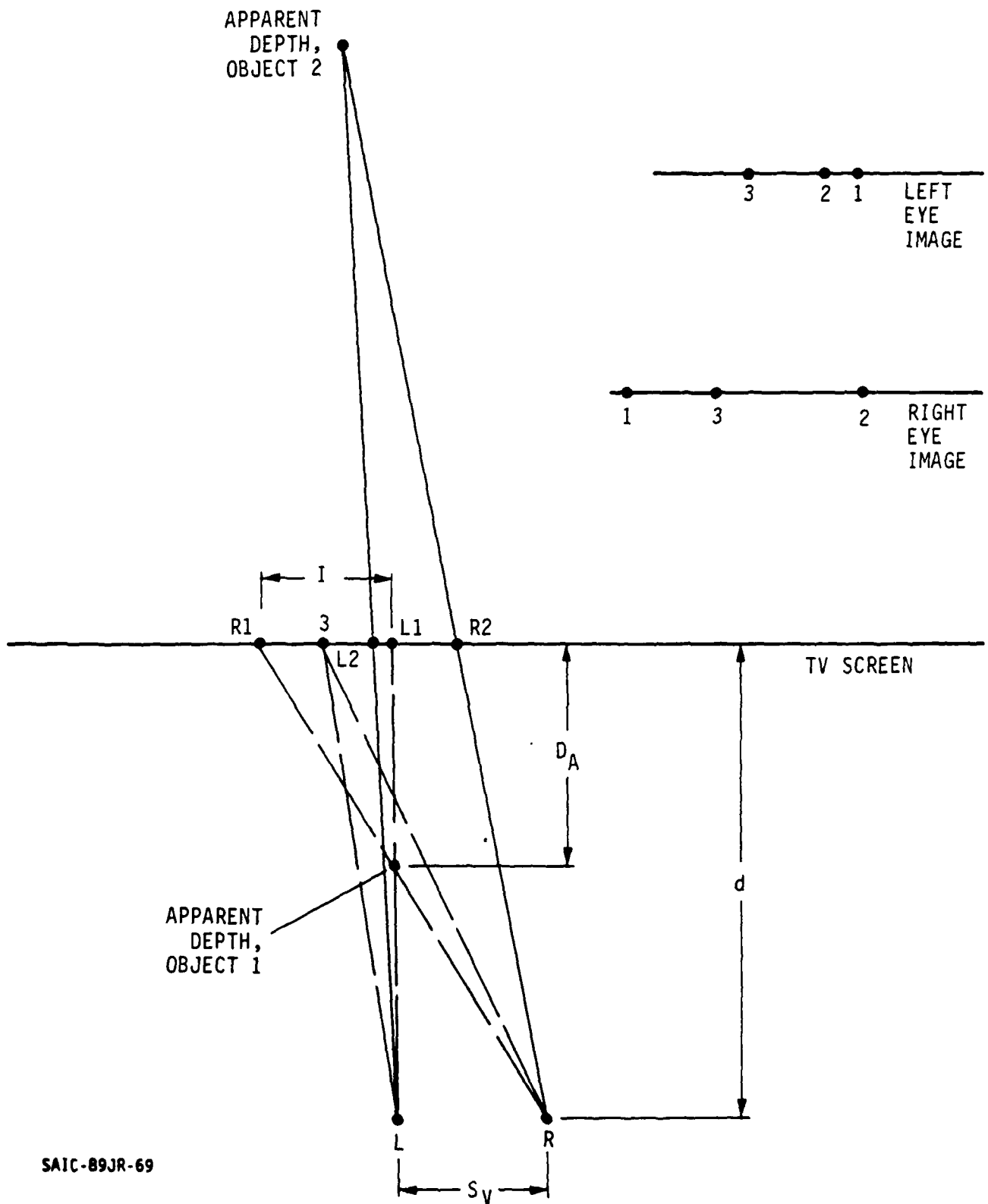
Figure 2-2. Viewing Geometry for Stereo Imaging. Three Objects are Shown
*on the TV Screen for both left (L) and right (R) eye Imaging. Object 1
is seen in the Stereo Image in Front of the Screen. Object 2 is
seen Behind the Screen. See Text for other Details.*

S_v = interocular distance, normally 2.75 inches (7 cm)

d = distance of observer from viewing screen

I = image separation on the viewing screen (shown for object 1)

D_A = apparent distance from the viewing screen for Object 1

A stereo-glasses equipped observer looking at the televised X-ray image sees the combined stereo image in such a way that some of the image detail appears to be in front of or behind the monitor screen, as shown in Figure 2-2. Three objects (dots) are assumed to be present in the scene. The relative positions of these dots on the screen for the right and left eyes are shown at the top of the figure. The eyes must adjust to bring the objects into registration. The eyes must focus in front of the screen to make the left-eye and right-eye images for Object 1 coincide, while the eyes must adjust to a focus behind the screen to make the eye images for Object 2 coincide. Object 3, since it is in the same location for both eyes on the screen, would appear at the surface of the TV screen. (It should be noted that if the images viewed by the eyes are interchanged, the apparent position of the objects change from the front to the back of the screen.) Using the principle of similar triangles applied to Figure 2-2, it follows that:

$$\frac{S_V}{I} = \frac{d - D_A}{D_A} \quad \text{then} \quad D_A = \frac{I * d}{S_V + I} \qquad \text{EQN. 1}$$

For a particular feature in the inspection object, having a depth, t,

$$D_A^t = \frac{I_t * d}{S_V + I_t} \qquad \text{EQN. 2}$$

The value of interest from the stereo view concerns the relationship between D_A and the actual depth of the detail in the object. If we define a new symbol, t_A, to be the apparent depth of a detail in the stereo-viewed image, then this apparent depth within the image is given by the relationship:

$$t_A = D_A^0 - D_A^t \qquad \text{EQN. 3}$$

where D_A^0 is the apparent distance from the viewing screen for the image of the inspection surface closest to the source, and D_A^t is the apparent distance from

the viewing screen for the image of a feature at an arbitrary depth, t, in the object. Substituting Equation 2 in Equation 3, we obtain:

$$t_A = \frac{I_0 * d}{S_V + I_0} - \frac{I_t * d}{S_V + I_t}$$

EQN. 4

This gives the relationship between the apparent depth (from the object surface) of the image feature at an actual depth, t, in the inspection object in terms of eye separation (S_V), viewing distance (d), and the separations of the surface image (I_0) and the t depth feature (I_t) on the viewing screen.

For a typical viewing situation, we can substitute actual values in Equation 4, as follows:

d = viewing distance = 61 cm

S_V = eye separation = 7 cm

I_0 = image separation on screen for a detail on the object
        surface, maximum value is 5 cm

Using these figures in Equation 4, we have:

$$t_A = 35.6 * \frac{(5 - I_t)}{(7 + I_t)}$$

As an example, if the separation of the image on the detector was 3 cm instead of 5 cm (as we have for a maximum image separation for a detail at the object surface), the value

$$t_A = 7.1 \text{ cm}$$

For this situation, the apparent distance of this detail at a depth, t, would appear in the stereo view to be 7.1 cm below the image of that of the object surface, or 18.3 cm from the viewing screen.

There is extensive literature on stereo imaging, but what is most important for a real-time X-ray stereographic system is depth perception. Depth perception from a stereo pair is accomplished, for the most part, with a monocular image presented to each eye; the two monocular images are shifted with respect to one

8

another in a specific way which results in a linear disparity between the two. This, in itself, is enough to yield the depth percept (what one perceives). As it turns out, disparity can only explain part of the phenomenon of stereo depth perception. Several additional qualities of the monocular images have been shown to affect depth perception, some to such a degree that they become dominant over disparity in defining the depth. Many of these phenomena cannot be explained in physical terms, since they are apparently psychological or biological effects. Whatever the explanation, however, the symptoms of these various effects are at least partially known, and some of them may affect the interpretation of stereo radiographs.

One such phenomenon is stereo capture.[11] Objects at one disparity which are enclosed within some contour or partial contour at another disparity will be perceived at the depth of the contour. This partial contour may consist of only corners, only edges, a broken contour, etc., and it can exist anywhere in the scene. The phenomenon has also been described as interpolation, which refers to the intermediate case where objects (or points, noise, surfaces, etc.) at one depth partially or fully enclosed within boundaries at another depth are perceived at some intermediate depth. Thus, the viewer interpolated between the two disparities to arrive at a result which is not necessarily present in the stereo pair. Stereo capture may significantly affect the radiographic view since cracks and flaws are expected to appear as contours or broken contours.

As part of this project, we have performed experiments to confirm the above phenomenon. A wire frame was placed at one depth in an object and, within the X-ray shadow of that frame, a single wire was placed at a different depth. These images were observed in stereo, and both the wire frame and the single wire appeared to be at the same depth. That, of course, was not the case; the eye was fooled, as indicated above. This did not influence the depth measurements for the two objects, as shown in Figures 2-3a and b. The depth- measurement procedure used in this case relates to the number of pixels the two images must be moved to make the images coincide. The amount of this movement is indicated by the white pixel shift numbers at the top of each illustration in Figure 2-3. For this discussion, however, we note that Figure 2-3a shows a relative depth of 23 when we bring together the two images of the single wire. Figure 2-3b shows a relative depth of 38 when we bring
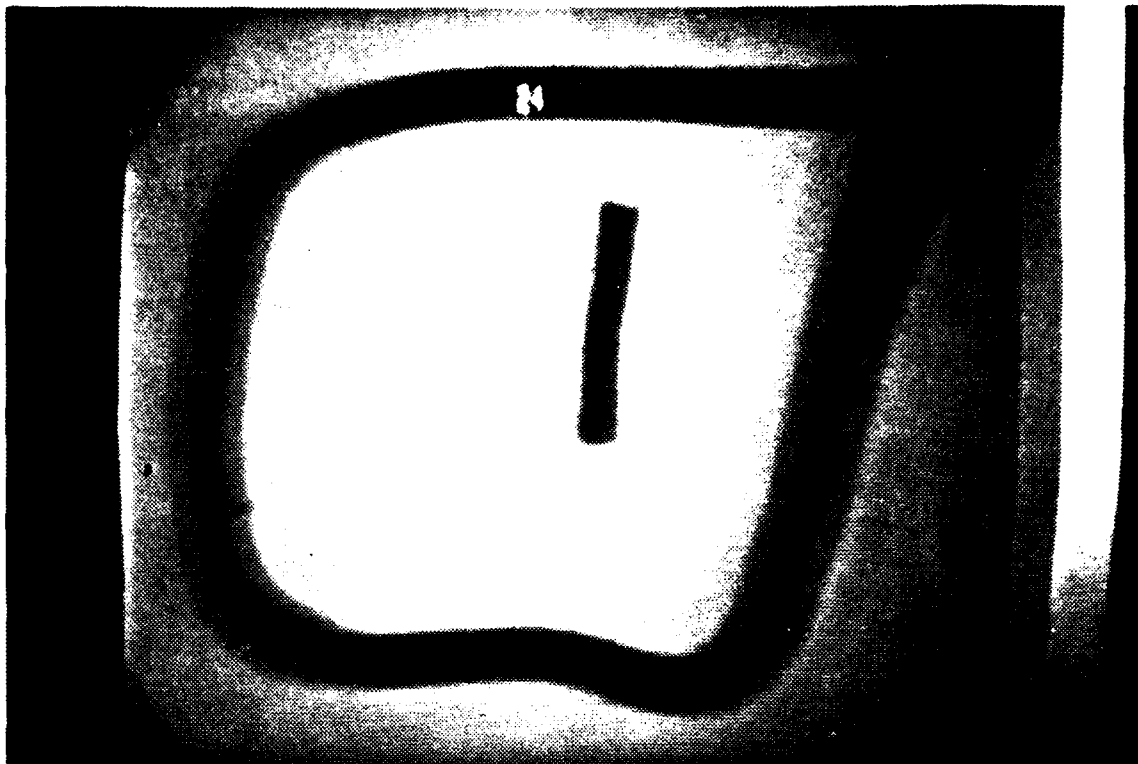
Figure 2-3a. Disparity Measurement on Inner Straight Wire. In the
Stereo View, the Straight Wire Appeared at the Same Depth as the
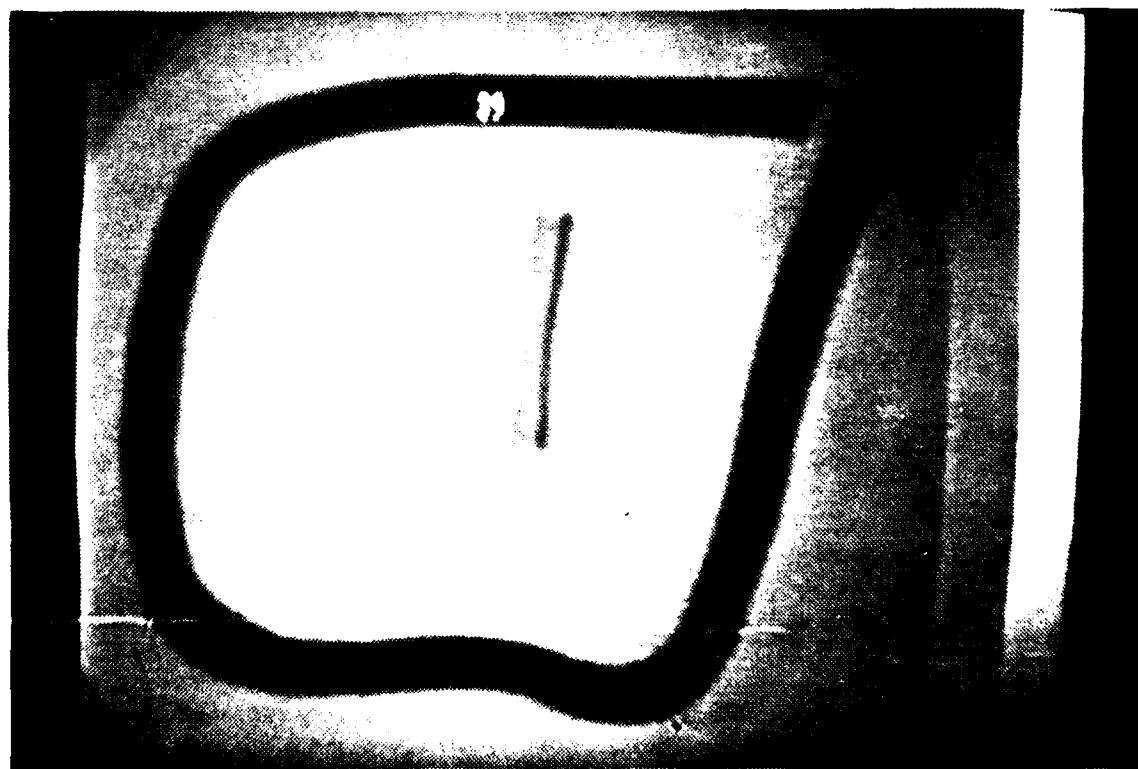Frame even Though the Actual Depth was Different.

Figure 2-3b. Disparity Measurement for the Wire Frame
Showing Depth Displacement.

SAIC-89JR-75

together the edges of the wire frame. Therefore, the two wire indicators are not at the same depth in the object. With calibration of the near surface and back surface, absolute depth measurement can be made.

2.2   X-RAY PROJECTION IMAGING AND DEPTH MEASUREMENT

It would be desirable to relate the apparent depth of an image detail to the actual depth of the detail in the object. To do that, let us consider the production of the stereo X-ray image as it would be accomplished if the X-ray focal spot moved between exposures. This is illustrated in Figure 2-4. In that illustration, we consider the following:

S = focal spot shift

L_2 = source-to-detector distance

t = depth in the object (distance from the object surface) of a feature

I_0^D = image separation at the detector for the two stereo views, for a feature on the object surface closest to the X-ray source, and

I_t^D = image separation at the detector for the two stereo views, for a feature at a depth, t, in the object.

Considering the similar triangles that meet at the detail at depth t in the object:

$$\frac{I_t^D}{S} = \frac{L_2 - L_1 - t}{L_1 + t}$$ EQN. 5

It follows that the geometric magnification, M_t, for the object detail at depth, t, is related as follows:

$$\frac{I_t^D}{S} = M_t - 1$$ EQN. 6

From Equations 5 and 6, the separation of the image at the detector for the two images taken by virtue of a focal spot movement, s, can be calculated. The image separation at the detector can be related to the image separation at the

11
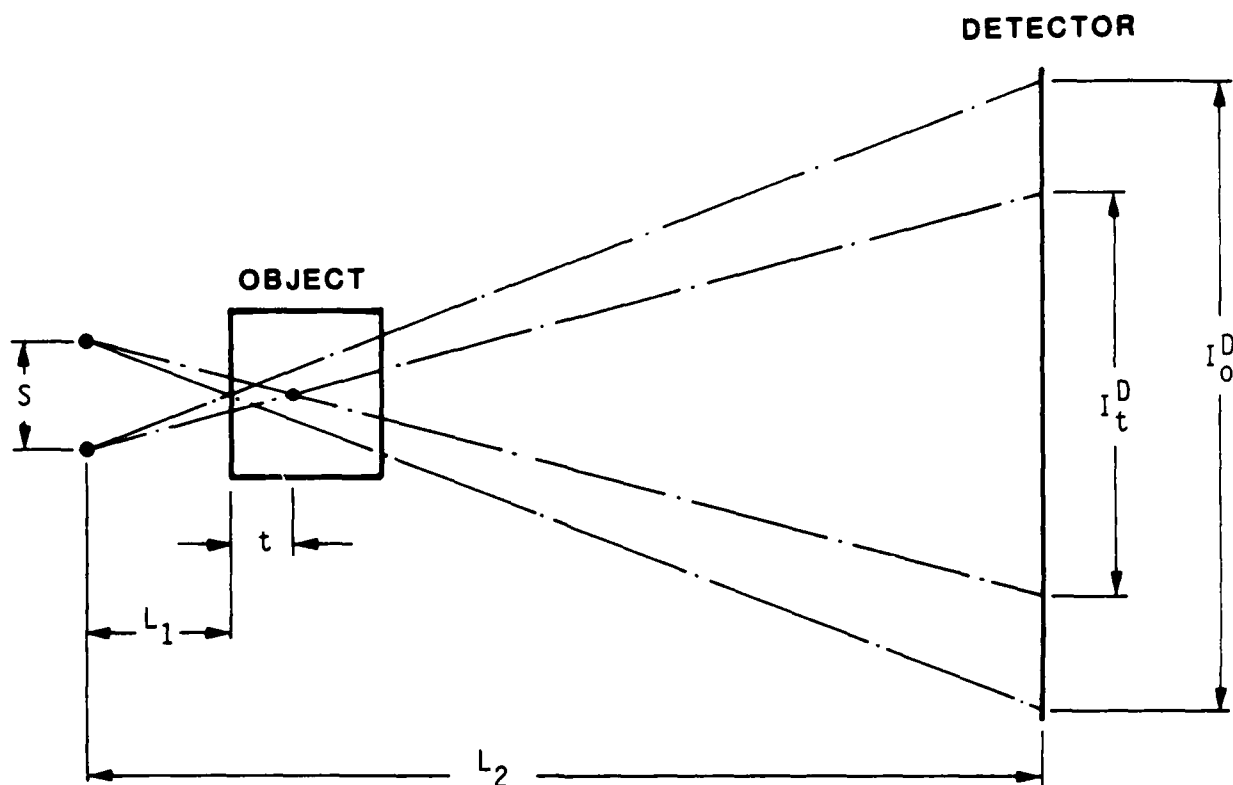
SAIC-89JR-65

Figure 2-4. Image Formation of Stereo Views for an X-Ray Focal Spot Shift, S. The Two Views of a Detail on the Object Surface are Separated at the Detector Plane by I_t^D. The Two Views of a Feature Having a Depth in the Object of t are Separated at the Detector by I_t^D.

viewing monitor. If we assume a conventional display, in which the detector diameter is displayed as the monitor diagonal size, then the relationship between the separation of the images at the detector, I^D, and at the monitor, I_t, is the simple ratio of the diameters. For the situation used in these experiments, the detector was a 9-inch (22.8 cm) diameter image intensifier. The television display was a 14-inch (35.6 cm) monitor. Therefore, the relationship between image separations for the stereo views was as follows:

$$I_t \cong 1.6 * I_t$$

This relationship and Equations 4, 5, and 6, permit us to relate image separation at the detector and monitor with the depth, t, of the image detail and the geometric magnification, M_t.

In the example illustrated earlier, a detail of depth, t, in the object had an image separation at the viewing monitor of I_t = 3 cm and an apparent depth for the stereo viewer, t_A = 7.1 cm. If we now relate this to the detector and the inspection object, assuming realistic values from these experiments as follows:

M_o = geometric magnification for the inspection object
surface = 10

L_2 = source-to-detector distance = 85 cm

L_1 = source-to-object surface distance = 8.5 cm

S = X-ray focal spot movement (putting values into
Equation 6) = 0.35 cm

then, from Equation 5,

$$\frac{I_t^D}{S} = \frac{L_2 - L_1 - t}{L_1 + t}$$

we obtain: t = 4.75 cm

Thus, the image separations at the detector and viewing monitor can be related to the actual depth in the object of an image detail. It should be noted that the geometric magnification of the image in the depth (or Z) direction is not the same as that in the X-Y plane. In this example, M_o = 10, so the X-Y plane at

the surface of the object is magnified 10x. The depth direction, however, using the above example, for a feature at depth t = 4.75 cm, is magnified only 6.4x. The magnification in the depth direction for the stereo view is smaller than the geometric magnification for the X-Y plane, and is not linear with respect to the depth of the feature in the object.

In papers[12,13] detailing the parameters in stereoscopic magnification radiography, Takahashi et al. have shown that:

$$S = \frac{S_V}{M} * \frac{(D - M*A)}{(D_V - M*A)}$$

where S = "ideal" focal spot separation

S_v = interpupillary distance

M = magnification

D = source detector distance

D_v = viewing distance

A = object thickness

This equation was derived for the particular case of equal longitudinal and transverse viewing magnification. A likely value for the object thickness, A, would be one inch (25 mm). Defects within the object would, of course, be much smaller.

Figure 2-5 shows a plot of the focal spot separation versus viewing distance for the A = 25 mm case. In this plot, we assumed a source detector distance of 1000 mm, and plotted curves at different magnifications. In the field trial, where S = 6 mm and M = 20, the optimum viewing distance was 800 mm. The observers were generally 750-900 mm from the television monitor. These values are consistent with the analysis above.

An important practical consideration relative to the recording and viewing geometrical parameters is depth resolution. At the outset, we must realize that depth resolution is dependent upon both geometrical and psychological factors;
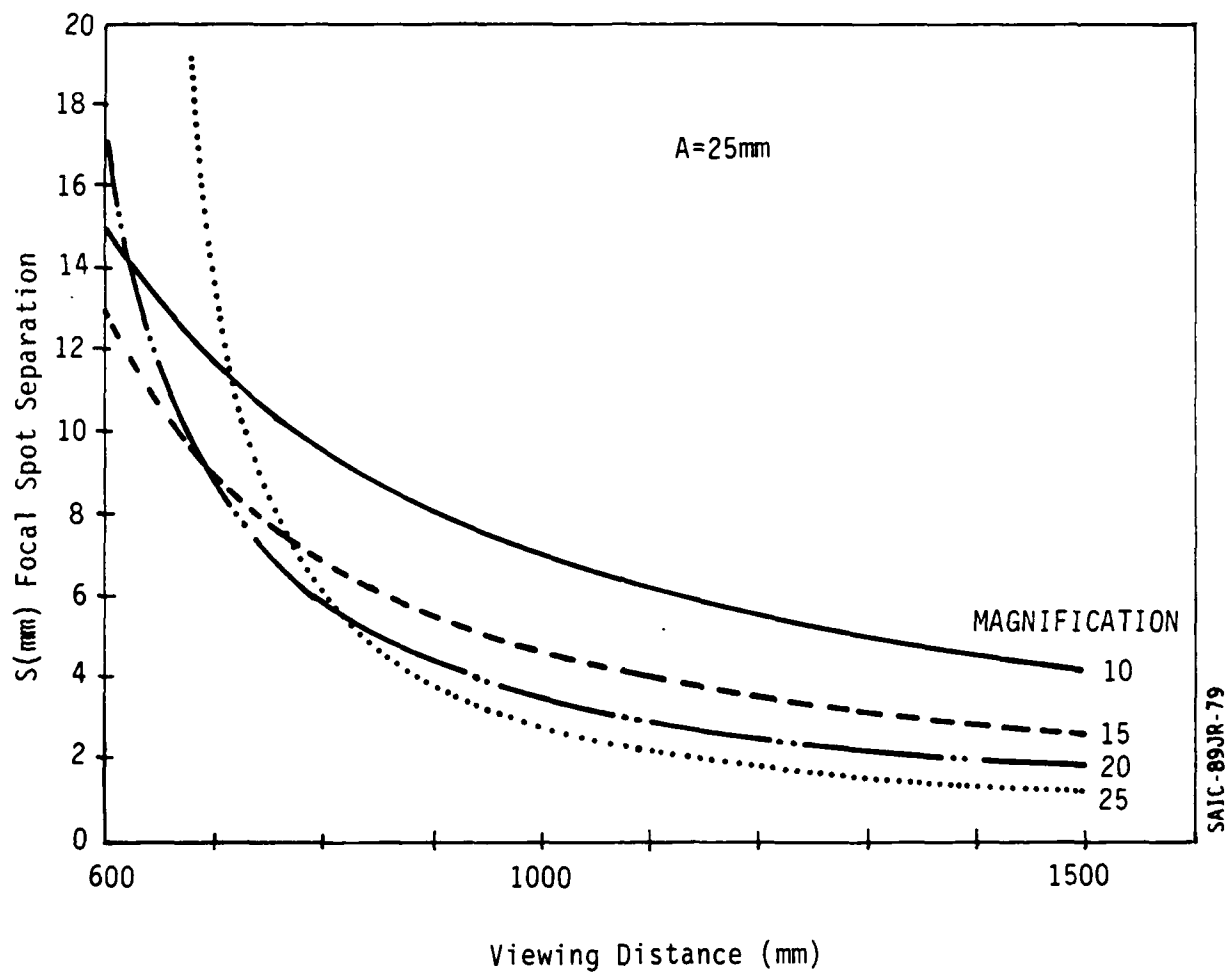
14

A=25mm

MAGNIFICATION

SAIC-89JR-79

Figure 2-5. Plot of "Ideal" Focal Spot Shift, S, Versus Viewing
Distance, D_V, for Equal Lateral and Depth Magnifications.

however, the geometrical considerations can provide an educated estimate, which will then be slightly altered for each viewer. To this end, we have extended the results of Takahashi[12,13] and derived the following two relationships for depth resolution element A (mm):

$$A_R = \frac{\Delta_R * D}{\Delta_R * M} + (M^2 * 5) \qquad\qquad \text{(a}$$

and

$$A_V = \frac{\Delta_V * D_V}{S_V * M} + (\Delta_V * M) \qquad\qquad \text{(b}$$

Here, A_v and A_r are the minimum resolvable depth differences detectable in an object when using the viewing and recording geometries defined above. Δ_R and Δ_V are the lateral resolution elements associated with the recording detector array and the viewing video monitor, respectively. We will treat a typical case (true in our experiments) in which $\Delta_V/\Delta_R = 24$, i.e., the CCD resolution element is 0.025 mm, and that of the video screen is 0.6 mm. The other parameters are also as defined below:

S = 2 mm; Focal spot separation

S_v = 63 mm; Interpupillary distance

D = 1000 mm; Source-detector distance

D_v = 800 mm; Viewing distance (constant only in Figure 2-6)

M = Magnification

The important quantity is, of course, A_v, since it represents the end product depth resolution which most directly affects defect detection capability.

Various algebraic manipulations of Equations a and b will yield important system capacities in terms of depth resolution. Two useful representations are depicted in Figures 2-6 and 2-7. In Figure 2-6, both viewing and recording depth resolution are presented as a function of the lateral resolution of the video component of the stereo RTR system. As expected, coarse lateral resolution yields

16

coarse depth resolution, with the coarsest case occurring at lower geometrical magnification. In Figure 2-7, the viewing depth resolution A_v (mm) is plotted versus the viewing distance D_v, with magnification the parameter. The recording depth resolution, A_r, is also treated as a parameter since it is not dependent on D_v. Note that, relative to Figure 2-6, the dependence is quite weak.

Figures 2-6 and 2-7 show that with reasonable stereo imaging and viewing parameters, the depth resolution element in the viewed image can be smaller than 1 mm. Moreover, 200-micron resolution in depth is possible if the system parameters are carefully balanced.

2.3   EQUIPMENT REQUIREMENTS

The schematic of a generalized inspection system for obtaining and viewing stereo X-ray images is shown in Figure 2-8. The components of the system that critically affect the quality of stereo-radiographic images will be discussed; specifically, the X-ray generator, X-ray detector, video camera, method of stereo viewing, and image processing.

2.3.1   X-Ray Source

One of the objectives of this study is the detection of discontinuities of the size of 25 μm or less in ceramic or composite materials. This requires geometric magnification to overcome the spatial resolution limitations of the typical X-ray image intensifier. The geometric unsharpness in the magnified image is given by $u_g = F(M-1)$, where U_g = geometric unsharpness, F = focal spot size, M = geometric magnification. Although the relationship between unsharpness and individual anomaly detection is not clearly defined, it is known that when the unsharpness equals or exceeds the dimension of the anomaly, contrast is greatly reduced. For the detection of 25 μm anomalies, the equation indicates that we can work at X-ray magnifications of 10-20 with X-ray focal spots of 1-2 μm.

The small focal spot size also provides a large depth of field in the magnified sample. In other words, the object is imaged clearly from front to back without excessive blurring due to geometric unsharpness.
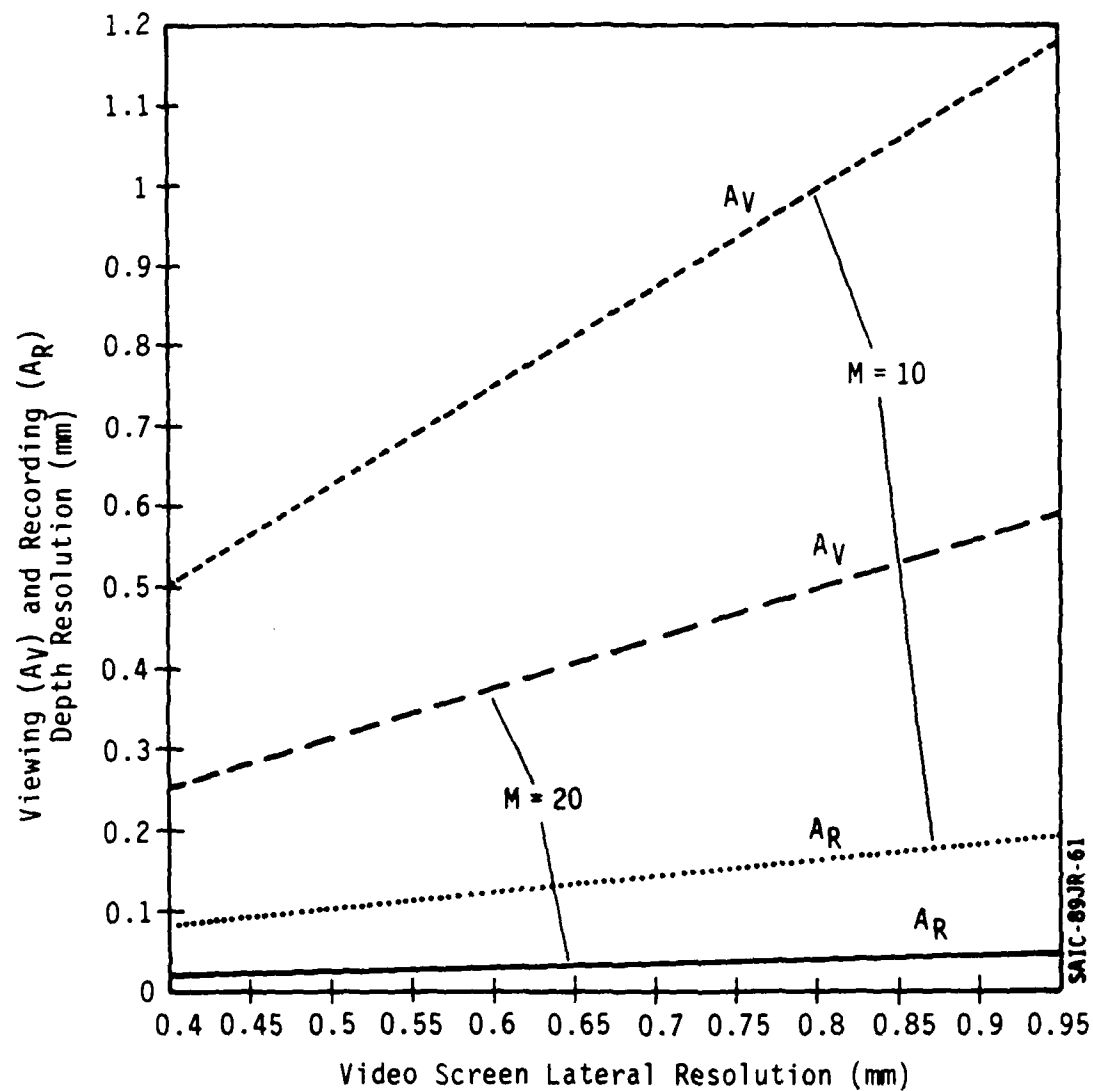
17

Figure 2-6.   Viewing and Recording Depth Resolution Versus Video Screen
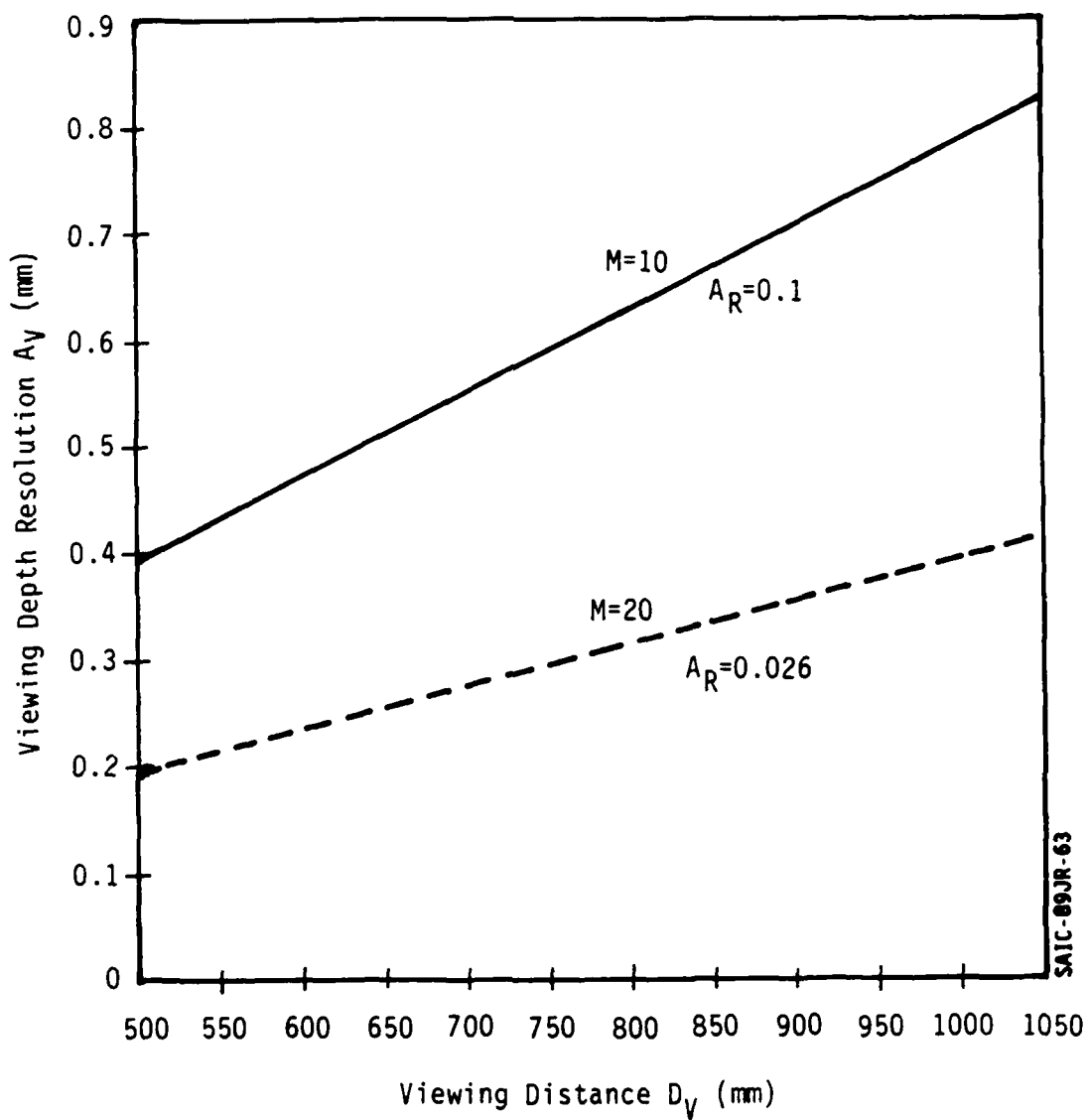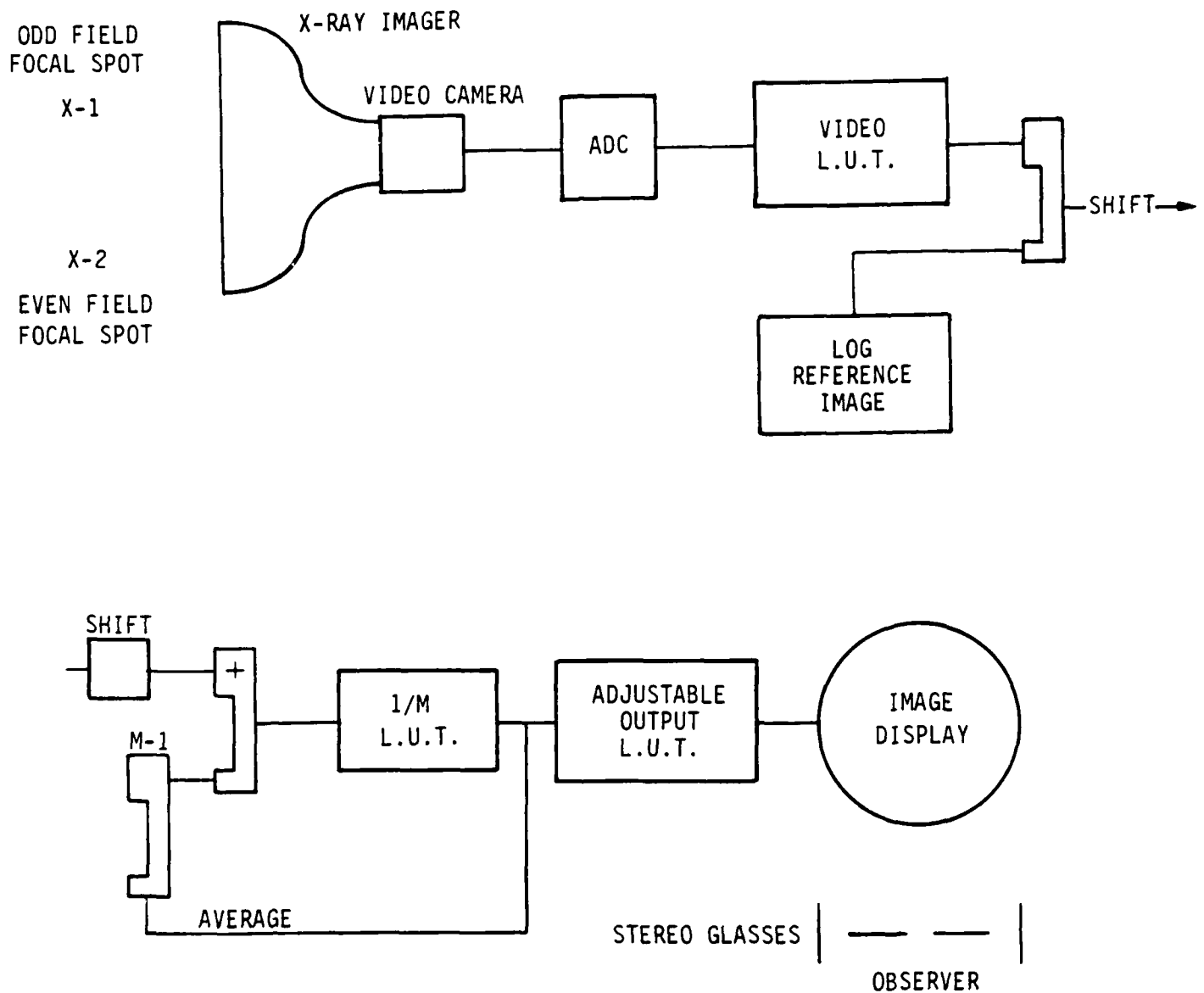Lateral Resolution.   Parameter M = Geometrical Magnification

18

Figure 2-7. Viewing Depth Resolution Versus Viewing Distance
for Parameters M = Geometrical Magnification and
A_R = Recording Resolution (mm).

19

X-RAY FOCAL SPOTS

ODD FIELD
FOCAL SPOT

X-1

X-RAY IMAGER

VIDEO CAMERA

ADC

VIDEO
L.U.T.

SHIFT →

X-2

EVEN FIELD
FOCAL SPOT

LOG
REFERENCE
IMAGE

SHIFT

+

M-1

1/M
L.U.T.

ADJUSTABLE
OUTPUT
L.U.T.

IMAGE
DISPLAY

AVERAGE

STEREO GLASSES

OBSERVER

SAIC-89JR-71

Figure 2-8. Flow of Information for a Real-Time Stereo
X-Ray Inspection System.

20

Two different views of the sample must be obtained for stereo viewing. The sample could be moved to obtain these two views; but moving the sample would require time, and would eliminate the possibility of stereo-viewing the object moving in real-time. Gross movement of the X-ray source would also provide the two views, but would have the same limitation. Fortunately, if a microfocus source is used along with geometric X-ray projection magnification, the movement of the focal spot required to generate a stereo pair is on the order of a few millimeters. This focal spot translation is within the range of magnetic deflection of the focused electron beam in a microfocus X-ray source. As will be discussed later, magnetic deflection of the electron beam can be made rapid enough to generate stereo pairs at video frame rates.

A limitation of the microfocus X-ray sources is their relatively low current levels, on the order of a milliampere maximum.

2.3.2 Imager

The relatively low current limits and, hence, low X-ray output of microfocus sources place some restrictions on the imaging system. The imager must have a high enough quantum efficiency and gain to make useful real-time images utilizing the limited flux. The imager must have sufficient resolution also. Fortunately, X-ray imagers exist which can do the job. One type is an X-ray-sensitive image intensifier. These imagers are large vacuum tubes that have a scintillator and photocathode sandwich which generate electrons under X-ray exposure. The electrons are electrostatically accelerated and focussed onto an output phosphor to generate a light image. The light image is then relayed with optics to a video camera. Alternatively, an imager made from a salt scintillator screen viewed with a low-light video camera could also work.

Whichever system is chosen, it must be "fast" enough to prevent smearing or ghosting in the images. If the time constant for the imaging system is too long, the image may not be completely extinguished between video fields. This would cause one field (and, hence, one of the stereo-pairs) to bleed into the other.

2.3.3   Display

A video monitor is required for viewing of the images. As with the imager, the monitor must have a small time constant as compared to the video refresh rate. Monochrome monitors usually have lower time constants than color ones. The monitor must also have high spatial and contrast resolution, needed for this real-time inspection application.

The stereo display concept for this project involves using the alternate video fields of an interlaced monitor to display the stereo-pair (see Figure 2-9). A standard RS-170 interlaced video monitor writes an entire "frame" to the screen in 1/30 of a second. The frame is actually composed of two "fields" interlaced together. The "odd" field is composed of lines one, three, five, etc. The "even" field is composed of the even lines. The electron beam writes one field, then returns to the top to write the second interlaced field. The field rate is 60 Hz.

If the position of the source of the X-rays is switched in synchronization with the field rate, then the two fields will display the two different views of the object. Because of the persistence of the eye, it appears that two images are present simultaneously, but displaced with respect to each other. In actuality, the monitor is displaying the left and right images of the stereo-pair alternately.

Light valve glasses, or other electro-optic shuttering techniques, can separate the two images so that only the left view is presented to the left eye, and vice versa. The shutter mechanism must also be synchronized to the video field rate and have a high light-extinguishing ratio.

ODD
FIELD

EVEN
FIELD

1
2
3
4
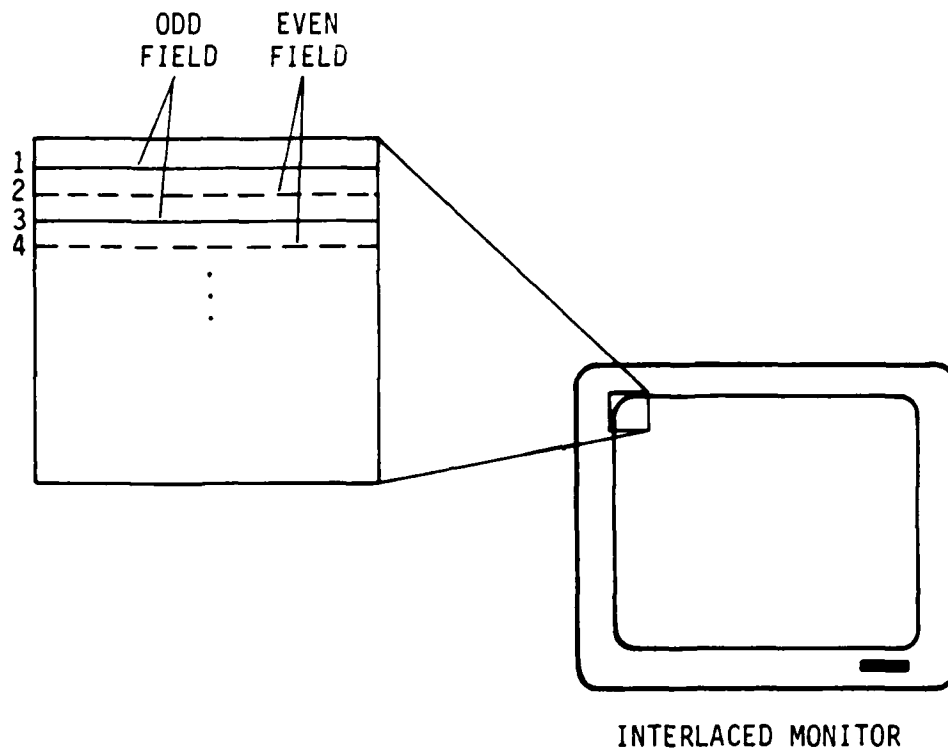
INTERLACED MONITOR

SAIC-89JR-73

Figure 2-9   Interlaced Video Display Scan Format.

## 3.0   STEREO-MICRORADIOGRAPHY SYSTEM DESIGN AND FABRICATION

3.1   MICROFOCUS SOURCES AND BEAM DEFLECTION

Two microfocus X-ray tubes were used during the project. One unit was a 90-kV Fein Focus X-ray system, and the second unit was a 160-kV unit manufactured by Ridge/IRT.

The 90-kV Fein Focus unit was used first in this project; the tube has a nominal focal spot less than 10 μm (range 3-200 μm). Lateral displacement of the electron beam in the microfocus X-ray tube has been accomplished by magnetic deflection to provide the different X-ray views for stereoscopic viewing. Beam focus has been maintained in this deflection (nominal 5-micron spot diameter). To produce the lateral beam deflection, a 1-inch-diameter by 3-inch-long aluminum extension tube was added between the normal (internal) steering/focusing coils and the transmission target (see Figure 3-1). The system was then refocused on the new target position. This extension tube provided the space needed to locate a pair of coils along the focused electron beam just before the target. This provided a means of magnetically deflecting the electron beam in either direction without measurably affecting the beam focus. A circuit was designed and built that made use of the "sync" pulse in the video signal from the electronic imager as a time reference to reverse the current in the coil pair so that the beam would be deflected. The "odd" field represents one X-ray view, and the "even" field represents another. The circuit schematic is shown in Figure 3-2 a, b, and c.

In other stereo experiments, use was made of a 160-kV IRT unit available at Sharpe Army Depot in Lathrop, California. This microfocus radiographic unit was used for the real-time inspection of many items in a depot situation. On this unit, the internal magnetic deflection system for the electron beam, which was part of the existing tube housing, was used for the beam displacement. Tests were conducted demonstrating that the internal deflection coils could be driven with suitable driver circuits, and that the response time of the internal deflection system was sufficiently fast to allow deflection at video rates. Most of the specific test sample applications to be discussed were performed with the IRT system. The driver circuitry is also shown in Figure 3-2.
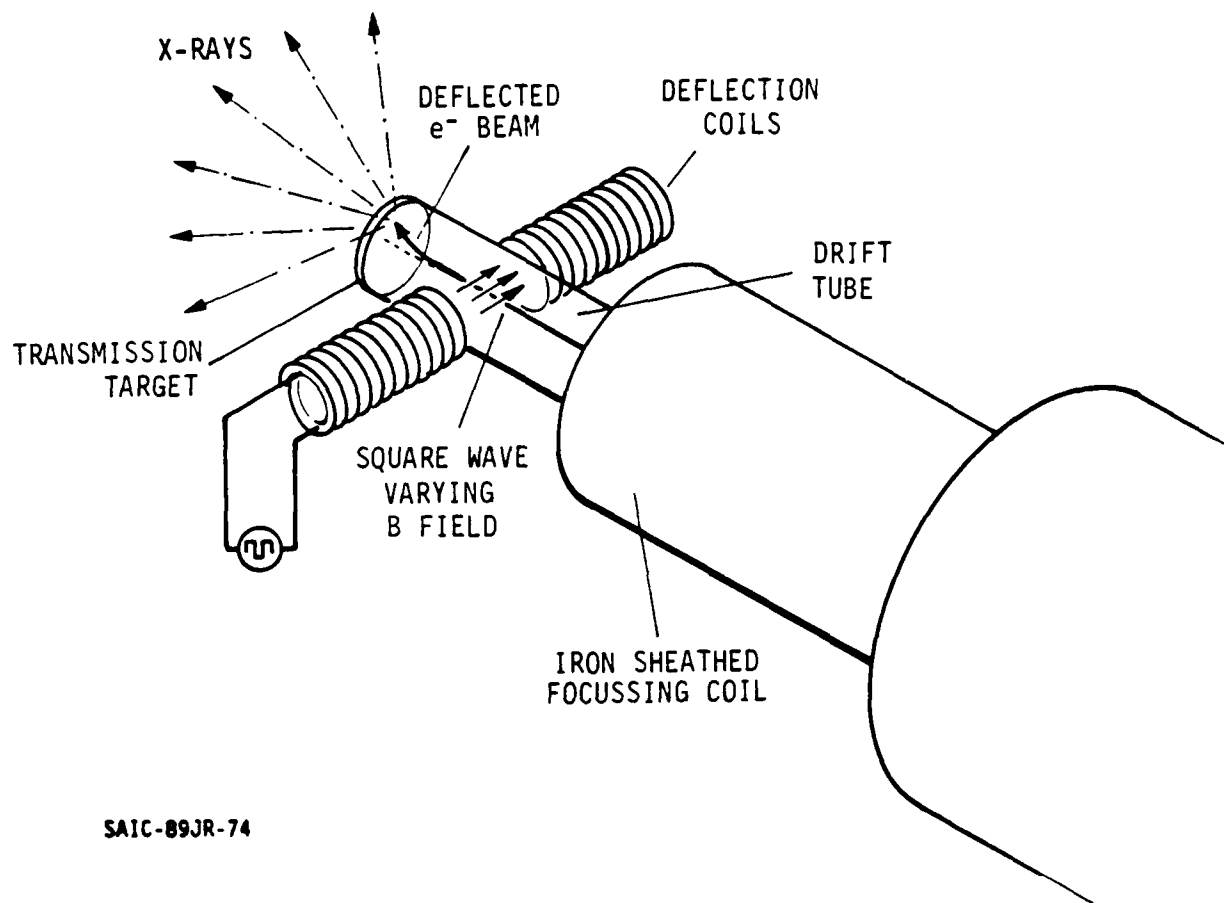
Figure 3-1.   Transmission Target Microfocus Beam-Deflection Geometry.
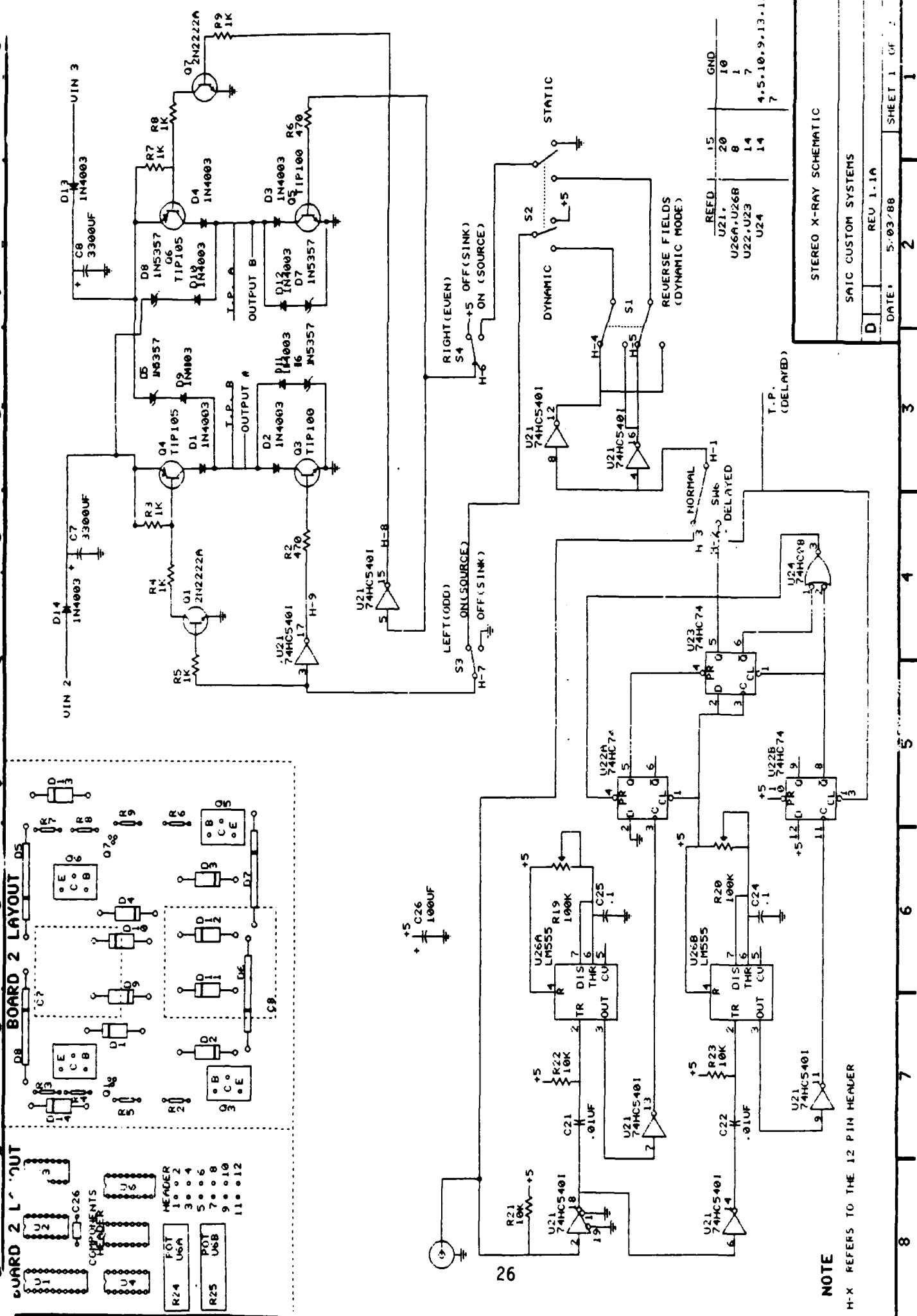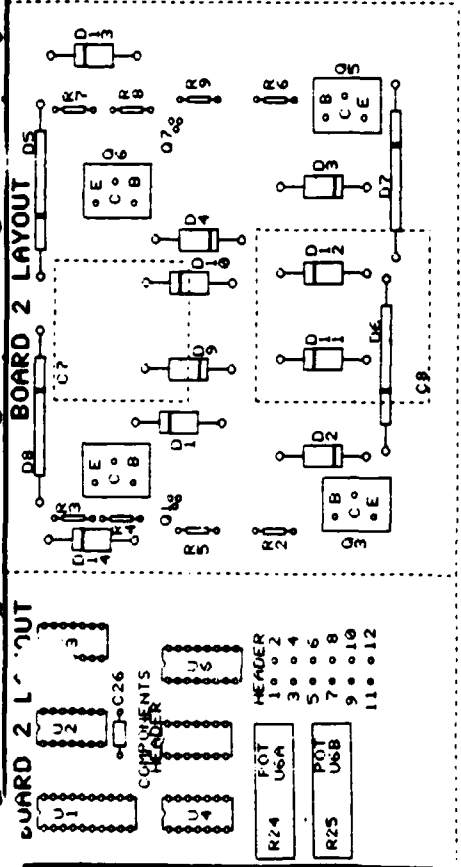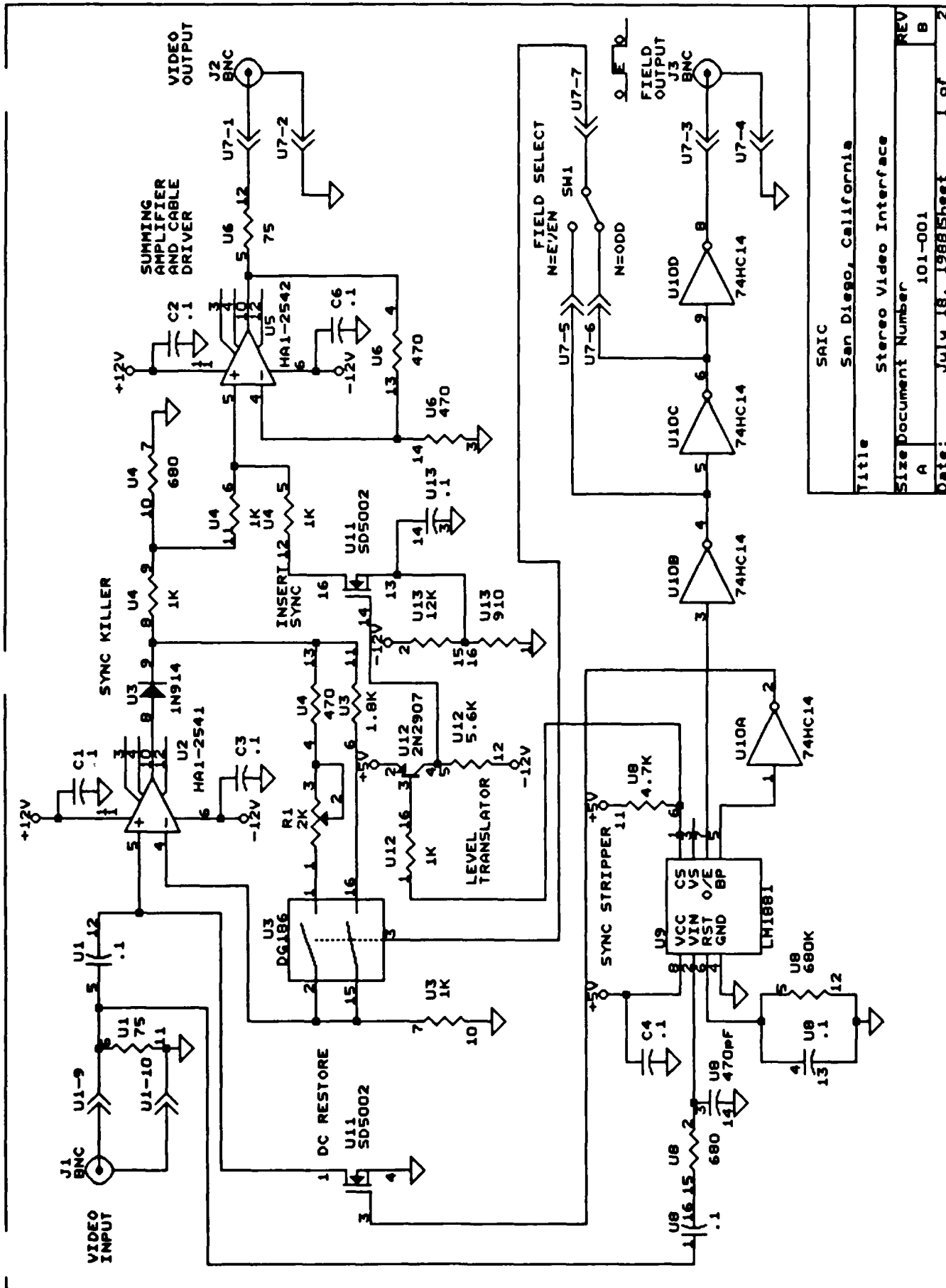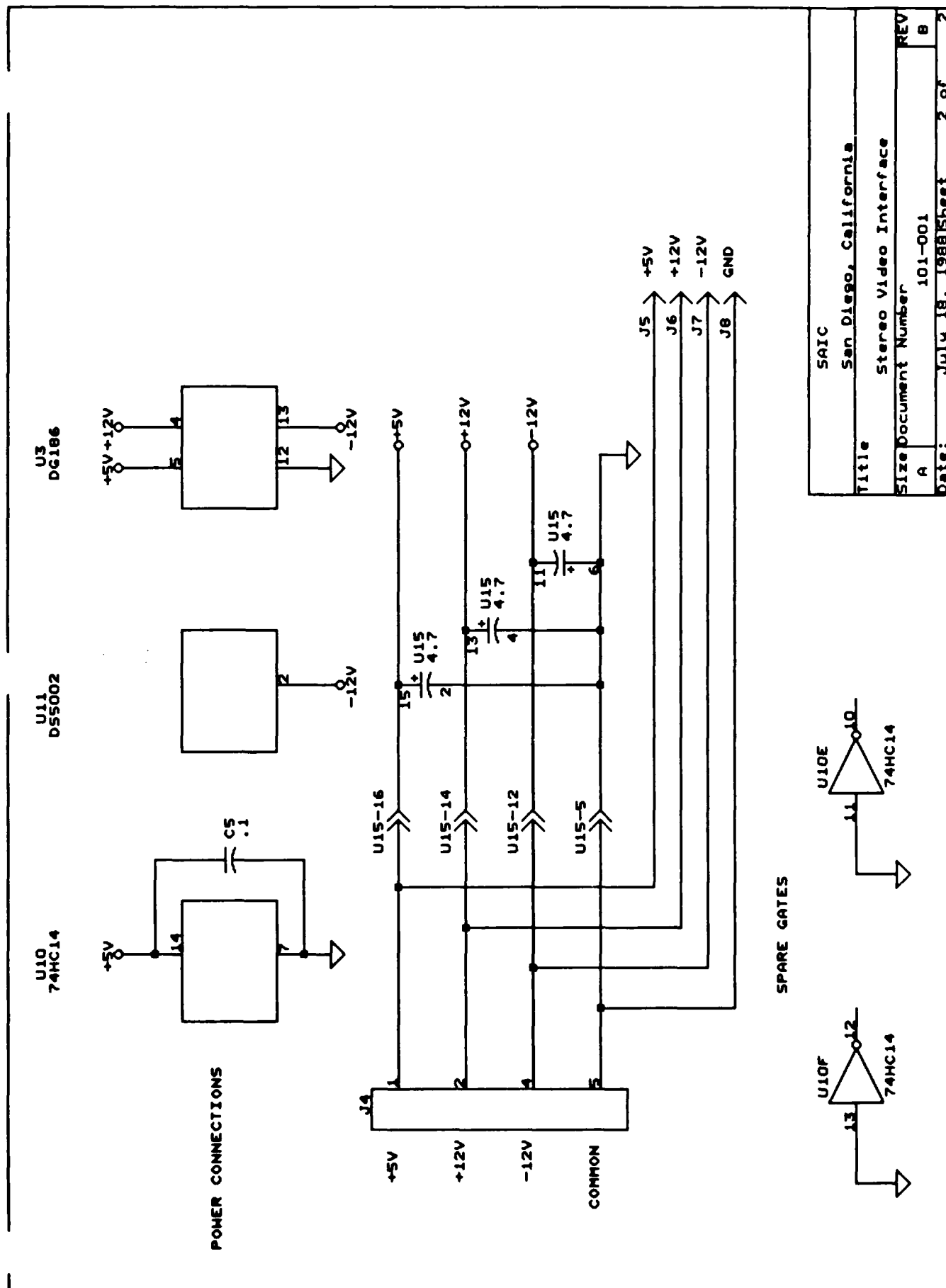
Figure 3-2a.

Figure 3-2b.

Figure 3-2c.

28

3.2   X-RAY IMAGER/CAMERA SYSTEM

The X-ray detector used throughout was an image intensifier, necessary because the microfocus units operate at low currents, and, therefore, relatively low X-ray output, when using the smallest focal-spot ratings. The Thompson X-ray image-intensifier tube is made up of a 9-inch-diameter CsI scintillator, a photocathode, and a 20-mm-diameter P-20 output phosphor. The CsI scintillator has a decay constant on the order of 1 μsec. The photocathode should be relatively fast also. The decay time for the P-20 phosphor is typically given in published literature as 0.5 msec.[14,15]

The first efforts with this system utilized a video camera with a plumbicon tube. Even though this is a relatively low-lag-time tube, the lag was found to be detrimental for this application. It was necessary to substitute a CCD camera for the plumbicon to produce images that did not show evidence of image persistence due to tube lag. This same kind of effect is evident on commercial television when a bright object is moved fairly rapidly across the video image. Unfortunately, artifacts tend to be more likely to affect CCD cameras than vidicon-type cameras. One needs a camera that has very low lag, good sensitivity, and low-light-level capability and reliability with few artifacts. The problem of tube lag is aggravated if one needs to go to even higher line rates than the 30 frames/second used in the present system. Suitable image processing may remove some of the poor characteristics described above.

3.2.1   TIME CONSTANT MEASUREMENTS

We have placed some emphasis on gaining insight on the origin of the image "ghosting" that is observed. The even/odd fields of each video frame contain the respective "right eye" and "left eye" stereo pair. These images should provide independent perspective views. We are observing a "bleeding" or "ghosting" of one image into the other; quantitatively, it appears to be about a 10% effect. Although the ghosting is somewhat distracting to the viewer, most observers quickly accommodate to the problem. We have studied several possible sources of the ghosting.

1) A synthetic stereo pair, one without ghosting, was fabricated using the image processor. This image was viewed through the Textronix polarizing screen. Virtually no bleeding was observed. The polarizing screen is not a major source of the problem.

2) Timing of the magnetic field reversal was varied with respect to the video-sync pulse. Table 1 summarizes the results of analyzing the video with the image processor. Ghosting can be reduced to about 7.5%, but not completely eliminated. This implies the ghosting is the result of improper magnetic-field switching or incomplete quenching of the image amplifier or video camera. We require complete extinction between video fields (1.2 ms).

TABLE 1

Ghosting as Function Field Switching Time

Magnetic Field Switched Prior to Sync Pulse (ms)	Observed Ghosting % of Total Signal
0	15
0.4	12.3
0.8	10
1.6	8.5
2.0	7.7
2.4	7.5
2.8	7.7
3.0	8.6
6.0	22.5

3) The following approach was used to measure the effective lag in the Thompson image intensifier tube. A lead (Pb) disk with a radial slit 0.5 inches long and 0.063 inches wide was used to chop the X-ray beam striking the image
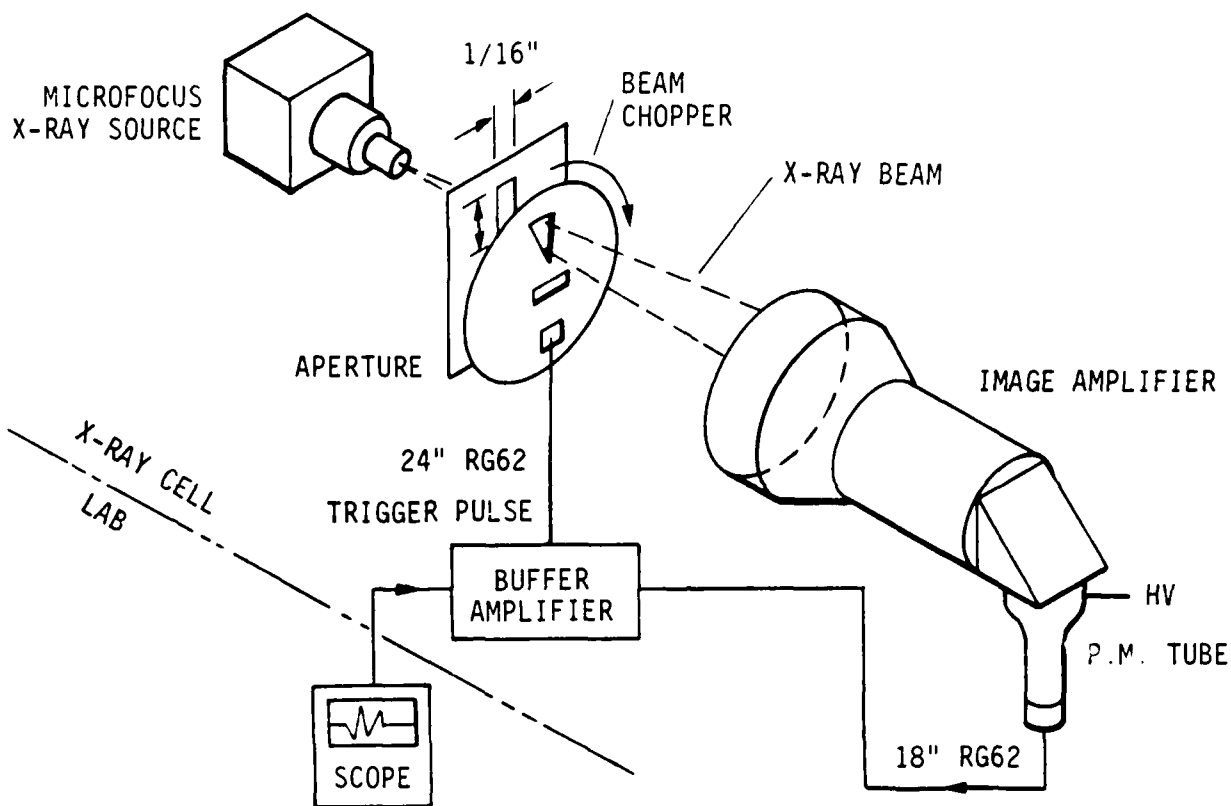
amplifier (IA) (Figure 3-3a). The time response of the experimental setup was verified by replacing the X-ray source with a light-emitting diode (LED). The image amplifier/photomultiplier tube (PMT) combination was replaced by the PMT (Figure 3-3b). Thus, the chopped-light pulse-source parameters (rise time, decay time) were measured directly by the PMT to confirm the needed response of the electronics. The observed image-amplifier persistence was confirmed and quantified. The output-response pulses for the PMT and the PMT/ image amplifier are shown in Figure 3-4. After analysis, the decay pulse was found to contain two or three components. A linear regression was used to fit the slow component, and we found that 10% +/- 2% of the pulse area (intensity) occurs after 1.2 msec, confirming the position that the image amplifier is the major cause of the "shadowing." This means that it may be necessary to select IA tubes for the stereo application or require the use of a faster output phosphor.
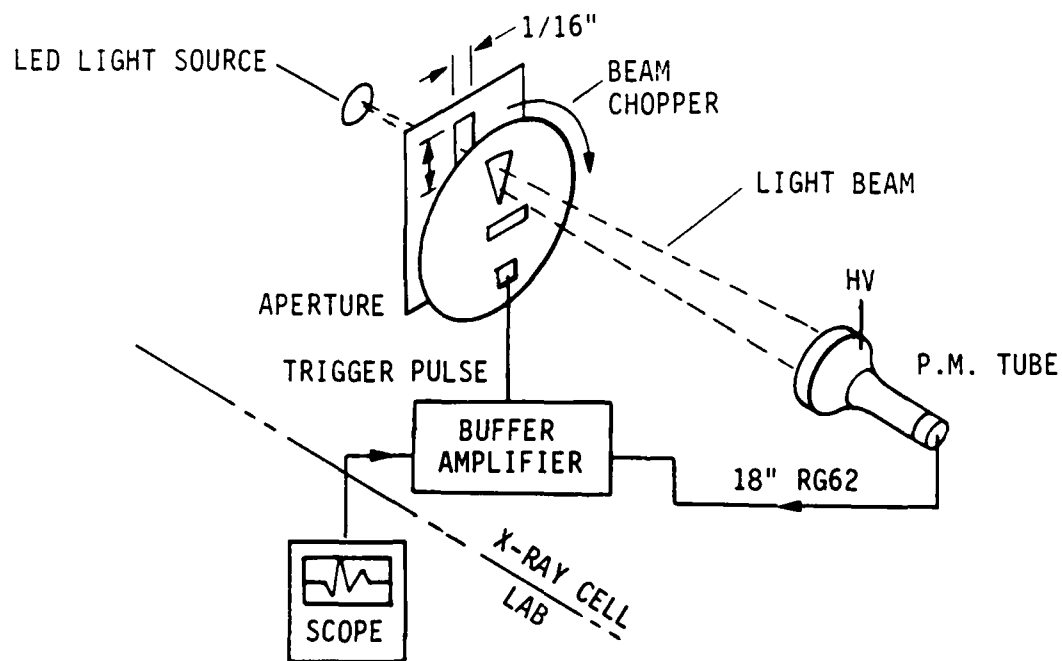
3.3   DISPLAY AND PROCESSING SYSTEM

There are many alternative possibilities for stereo-viewing of the televised X-ray images. These include various multi-camera, multi-television monitor and mirror systems to present stereo-viewing capability for commercial or scientific television. Several systems have been described in the Proceedings of a Conference on Three-Dimensional Imaging.[16] A good review of stereo-television systems has been presented by Butterfield.[17] A new viewing system employing dual liquid crystal display units in a helmet arrangement is currently under development by NASA.[18]

Two stereo-viewing systems were evaluated, one manufactured by Honeywell and a later development manufactured by Tektronix. This later development turned out to be markedly superior for our use in viewing stereo images generated by X-ray. The decision was made to use the Tektronix Model SGS 410 stereoscopic 3D display unit. This unit consists of a large liquid- crystal stereoscopic modulator that is mounted across the front of the television monitor. This modulator, controlled from a driver unit, provides right and left circularly-polarized light transmission for alternate television frames or fields. A viewer wearing appropriate glasses sees the alternate set of images with each eye, thereby providing stereo-viewing capability.

31

1/16"

MICROFOCUS
X-RAY SOURCE

BEAM
CHOPPER

X-RAY BEAM

APERTURE

IMAGE AMPLIFIER

X-RAY CELL
LAB

24" RG62
TRIGGER PULSE

BUFFER
AMPLIFIER

HV

P.M. TUBE

SCOPE

18" RG62

a.   Data Collection Configuration.

1/16"

LED LIGHT SOURCE

BEAM
CHOPPER

LIGHT BEAM

APERTURE

HV

P.M. TUBE

TRIGGER PULSE

BUFFER
AMPLIFIER

18" RG62

SCOPE

X-RAY CELL
LAB

SAIC-89JR-72

b.   Test Configuration.

Figure 3-3.   Measurement of Effective Decay Constant for Image Amplifier.

32

MEASUREMENT OF PHOSPHOR DECAY TIME

Science Applications International Corporation ®

INDUSTRIAL QUALITY INC

CHOPPED X-RAY SOURCE – IMAGE AMPLIFIER OBSERVED WITH PMT
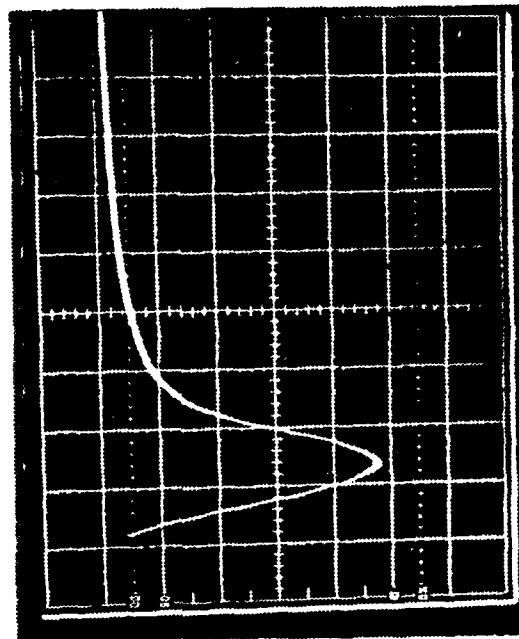
0.1 V/DIV

0.2 msec/DIV

PULSE SIGNIFICANTLY BELOW BASELINE AFTER 1.4msec

CHOPPED LED LIGHT SOURCE – OBSERVED WITH PMT

20 mV/DIV

0.2 msec/DIV

PULSE RETURNS TO BASELINE WITHIN 0.4 msec

SAIC-88JR-14

Figure 3-4.

33

The Tektronix stereo-viewing system is shown in Figure 3-5. Figure 3-5a shows, in simplified form, the television monitor (left) with the relatively flat modulator panel mounted over the television monitor screen and the viewer's special glasses. Figure 3-5b shows the actual "hardware" mounted on the video monitor. A viewer wearing the special glasses is at the right. Clip-on models of these are available for viewers with refractive corrective glasses. The advantages, as compared to the Honeywell light-valve glasses, include the following:

1. Less restrictive: no wires attached to viewer, normal room-vision capability.

2. More convenient: wearer uses normal-appearing glasses, and can see other objects in the viewing room.

3. More brightness reaches the viewer: less potential for loss in stereo-image contrast.

A low-persistence, high-resolution monochrome monitor was used to display the images. Included in the beam-deflection circuitry was a video- field balancing circuit. This circuit was used to make the brightness of the two fields equal to avoid annoying interfield flicker.

At the SAIC facilities, a Trapix 5500 image processor was available for use on this project. The image processor was used to contrast-stretch the images in real-time. Quantitative depth measurement was performed on the Trapix 5500 off-line. Also, off-line, various convolutions could be applied to the images. At Sharpe, a Matrox-based image processor was used as a frame grabber and storage device.

3.4   RECORDING AND STORAGE

Real-time images were recorded on three-quarter-inch video tape. It worked equally well whether the beam-deflection circuitry was energized and producing displaced interlaced images or during conventional real-time inspection. During playback, the sync signal from the tape was used to synchronize the stereo-glasses for dynamic three-dimensional viewing.
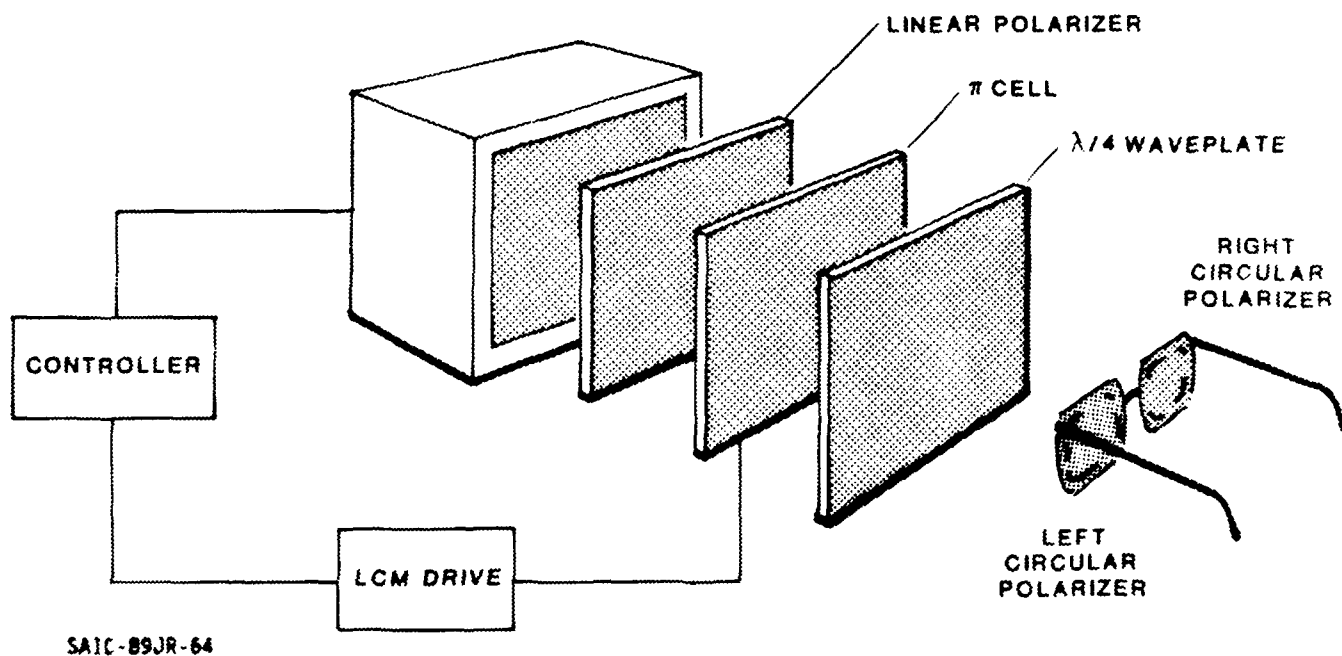
34

LINEAR POLARIZER

π CELL

λ/4 WAVEPLATE

RIGHT CIRCULAR POLARIZER

LEFT CIRCULAR POLARIZER

CONTROLLER

LCM DRIVE

SAIC-89JR-64

Figure 3-5a.

Figure 3-5b. Photo of Tektronix SGS 410 Stereoscopic 3D Display System. TV Monitor with Stereoscopic Modulator Panel is at the left.

35

When image processors were used, full frames or displaced fields could be stored digitally. The processed images were stored on either the computer's hard disks, removable bernoulli disks, or floppies. Afterwards, the images could be transferred to another computer over a communication link or by direct transfer of media.

3.5   SAMPLE MANIPULATOR

There is one problem associated with microfocus projection radiography. A large X-ray magnification means a limited area (volume) of inspection. This can be partially offset by compromises in magnification with the ability to switch to higher magnification when necessary. A sample manipulator permits scanning, which also offsets the limitation of a limited field of view.

A sample manipulator was built for this project. Three linear translation tables were mounted together to afford an xyz translation capability. The tables were driven by d.c. motors. A rotation table was mounted on the vertical, z translation stage to provide for rotation of the samples. Figure 3-6 shows a photograph of the sample manipulator in use. The X-ray image amplifier can be seen in the background.

The manipulator not only allowed for scanning of the entire volumes of the samples during the real-time inspections, but it also provided remote control over the geometric projection magnification value.

3.6   OPERATOR CONTROLS

A small operator console was built for ease of operation of the system. The manipulator motor drivers, the beam deflection circuitry, and the video field display and balance circuitry were housed in the operator console. All controls were mounted on the console's front panel. A photograph of the operator console is shown in Figure 3-7.

The X-ray sources had their own control panels or consoles. The video display was self-contained. Image processing was controlled via computer.
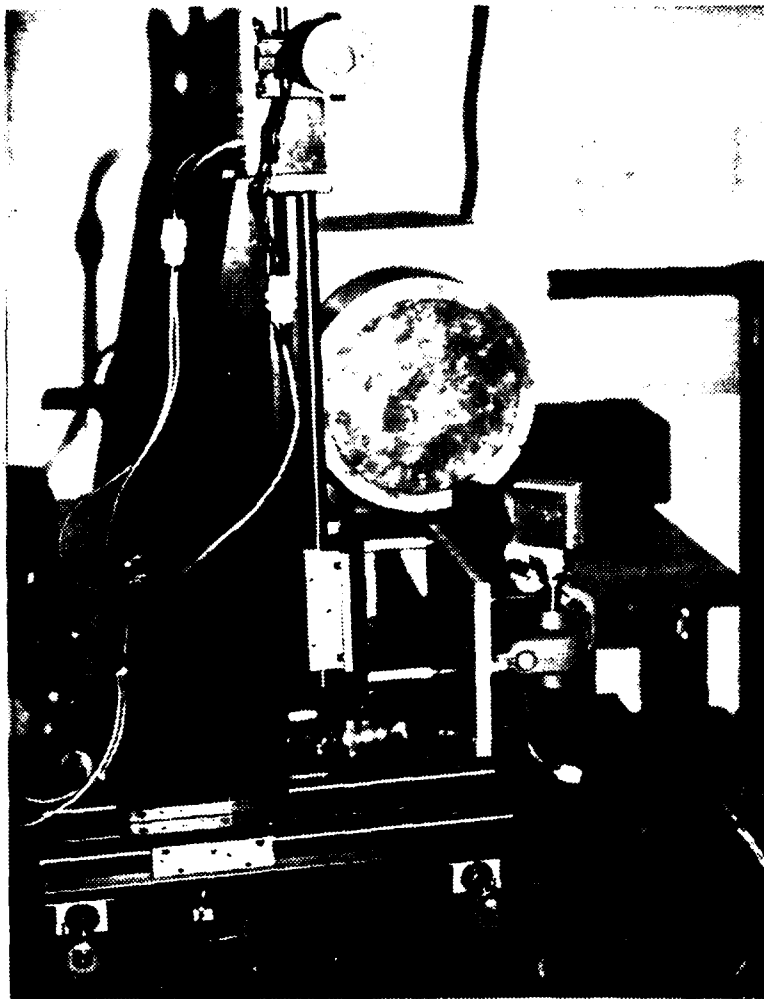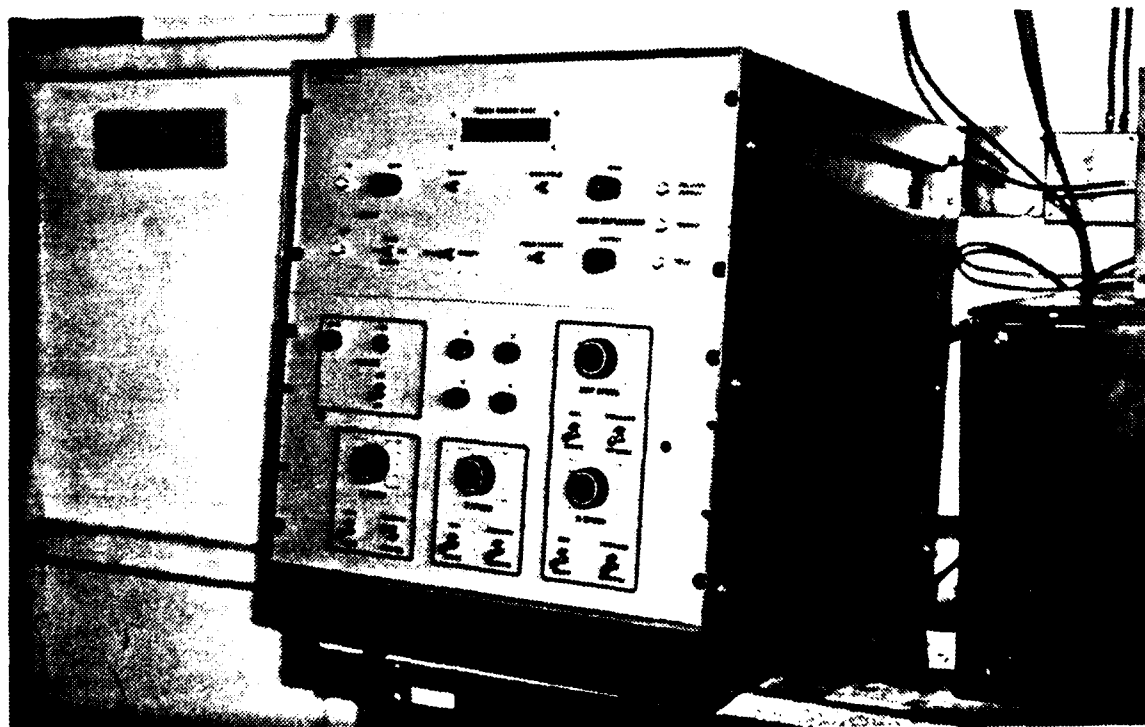
Figure 3-6.
Four Axis Manipulator.

Figure 3-7.   Stereo Microradiographic Beam Deflection
Control and Manipulator Control.

4.0 SYSTEM PERFORMANCE AND RESULTS

4.1 VISUAL PERFORMANCE ASSESSMENT

The stereo-microradiography system produced high-resolution dynamic stereo images. Comfortable viewing of samples in motion with depth perception was obtained. By varying system parameters, the amount of depth perception and the perceived location of the object could be varied. The images could be made to appear in front of or behind the monitor by switching right to left fields. One presentation is always preferable, though, because it is consistent with the other depth clues from image magnification. The sense of the fields could be switched in order to make close objects (which are magnified more) appear to be toward the observer.

In reconstructing the images for stereo viewing, it was found that the physical separation of the two stereo images on the viewing screen could not be made arbitrarily large. If the separation is too large, it becomes difficult (or impossible) for observers to force their eyes to converge at the proper distance. A comfortable and practical viewing system involved viewing the reconstructed stereo views on a 14-inch (35.6 cm) television monitor at a viewing distance of 2 feet (61 cm). (This viewing distance is about 3x the picture height, a value within normal limits, as determined by experiments with television viewing. See Ref. 19.) For a maximum image separation on the monitor of 2 inches (5 cm), the closest object to be focused was about 10 inches (25.4 cm) in front of the viewing screen (14 inches, 35.6 cm, from the observer). This could be done by all observers tested.

4.2 QUANTITATIVE DEPTH MEASUREMENT

4.2.1 Computer-Aided

As previously indicated (see Section 2.2), depth assessments can be made from the stereo image pair. The left and right fields produce a double image on the display when viewed without the synchronization produced by the polarizing system. One field is slightly displaced relative to the other. The degree of this displacement depends on both the magnification and the beam deflection. Similar
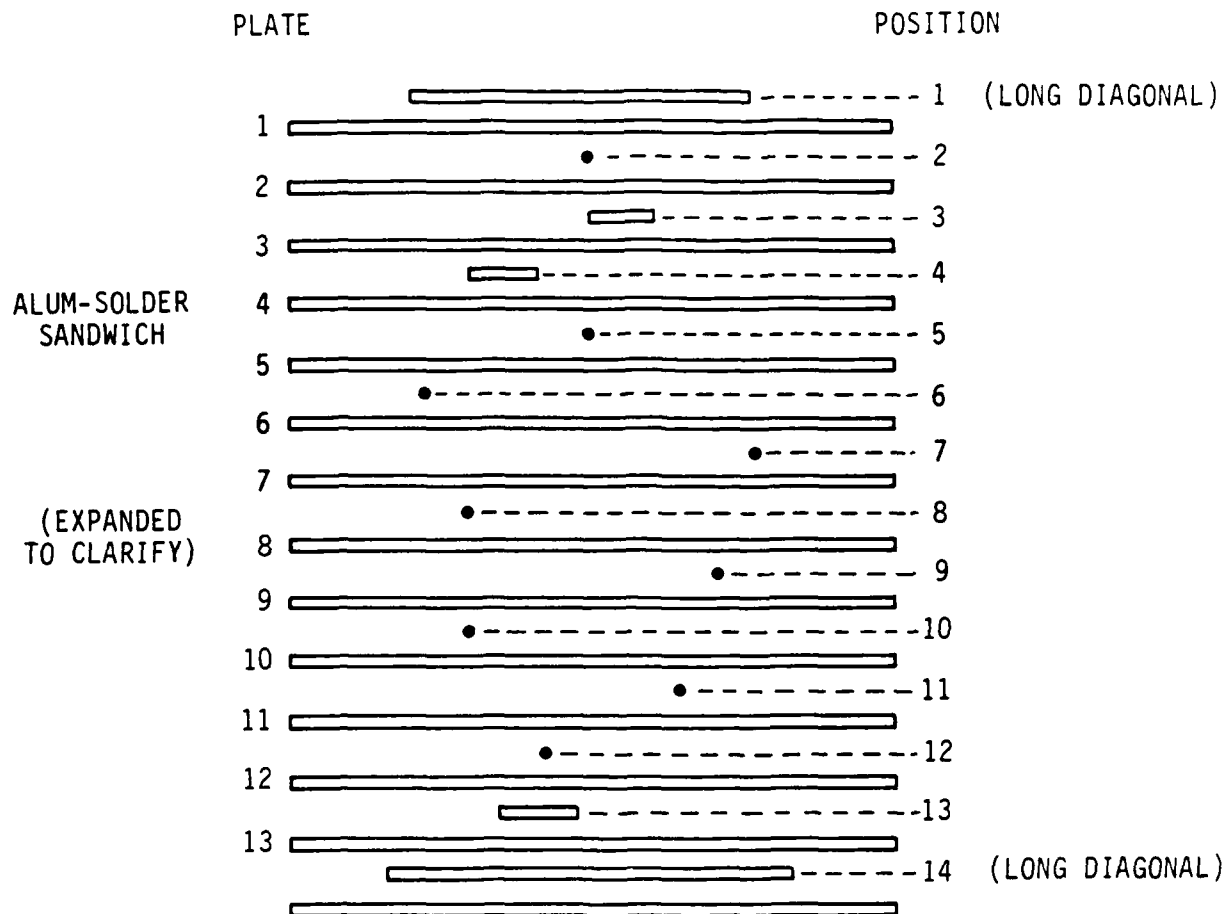
objects (points, pixels) on the two images exhibit parallax or image disparity. The degree of disparity represents the "depth" of the discontinuity in the object. Methods are available for measuring this disparity. A simple approach is to scale the disparity on the display. This gives a relative measurement of depth, but it is not very accurate. A better approach is to identify the pixel separation for the display for corresponding points in the two images. A readout of the pixel position in the horizontal direction, which is how the disparity is displayed, produces a pixel "shift" which can then be related to the depth.

One depth-measurement method applied in this project is to "scroll" one image over the other until the corresponding pixels overlap, using a trackball. The pixel shift required to do this is readily displayed on the monitor.

Whether parallax or magnification is measured, the depth determination requires suitable calibration. This can be achieved with fiducials on, e.g., the front and rear face of the object or at suitable distances in the "Z" direction. In any case, calibration is not expected to be a very difficult task, particularly for inspections made in a fixed-geometry arrangement. Of more concern is knowing where the "edges" of a flaw are located. These generally tend to show some unsharpness. Suitable image processing can aid in this case. Edge-enhancement techniques will be of use in defining edges more precisely. In addition, a two-cursor display, with the axis positioned at exactly corresponding points in the two images, could allow more precise parallax determinations.

Several samples were tested using the approach just described, and the method is feasible. Figure 4-1 shows one of the test objects made up for this test. The results of the pixel-shift measurement are shown in the table. Two discrepancies are noted. The reason for this may be wrong identification of the wire in the images, or that they were near the edge of the field of view and, therefore, subject to distortions.

Another depth-measurement technique involved the generation of a stereo pair for a movable video-overlay cursor. The "3D" cursor could be moved laterally or in the depth direction as the operator was viewing the images in stereo. A continuous depth-measurement value was displayed for the cursor. When the cursor

PLATE   POSITION

                                                    — 1 (LONG DIAGONAL)
1
                                                    — 2
2
                                                    — 3
3
                                                    — 4
ALUM-SOLDER   4
SANDWICH   — 5
5
                                                    — 6
6
                                                    — 7
7
(EXPANDED   — 8
TO CLARIFY)   8
                                                    — 9
9
                                                    —10
10
                                                    —11
11
                                                    —12
12
                                                    —13
13
                                                    —14 (LONG DIAGONAL)

13-ALUM, PLATES
   .050"x2x2   X-RAY
                                                SOURCE
14-LENGTHS WIRE SOLDER
        .025" DIA

POSITION	MEASURED PIXEL SHIFT (PARALLAX)	DIFFERENCE RELATIVE TO POSITION #1	CALCULATED VALUE (PIXEL)
P-1	30	0	0
2	32	2	2.3
3	33	3	4.6
4	34	4	6.9
5	38	8	9.2
6	41	11	11.5
7	52	22	13.8
8	45	15	16.1
9	51	21	18.5
10	49	19	20.7
11	53	23	23.1
12	52	22	25.4
13	59	29	27.7
14	60	30	30

SAIC-89JR-67

Figure 4-1a. Stereo Depth Measurement Test Specimen.
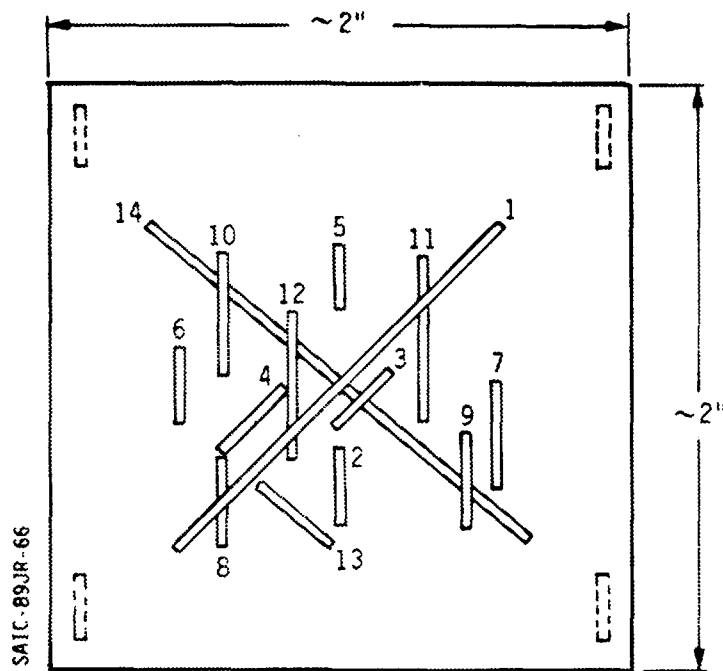
Figure 4-1b. Orientation of Wires (Solder) on Aluminum Plates
Stacked as in Figure 4-1b The Wire Lengths Varied as Indicated.
Wires Shown in the four Corners were Placed to Prevent Skewing
of the Plates. View as Seen by X-ray Source.
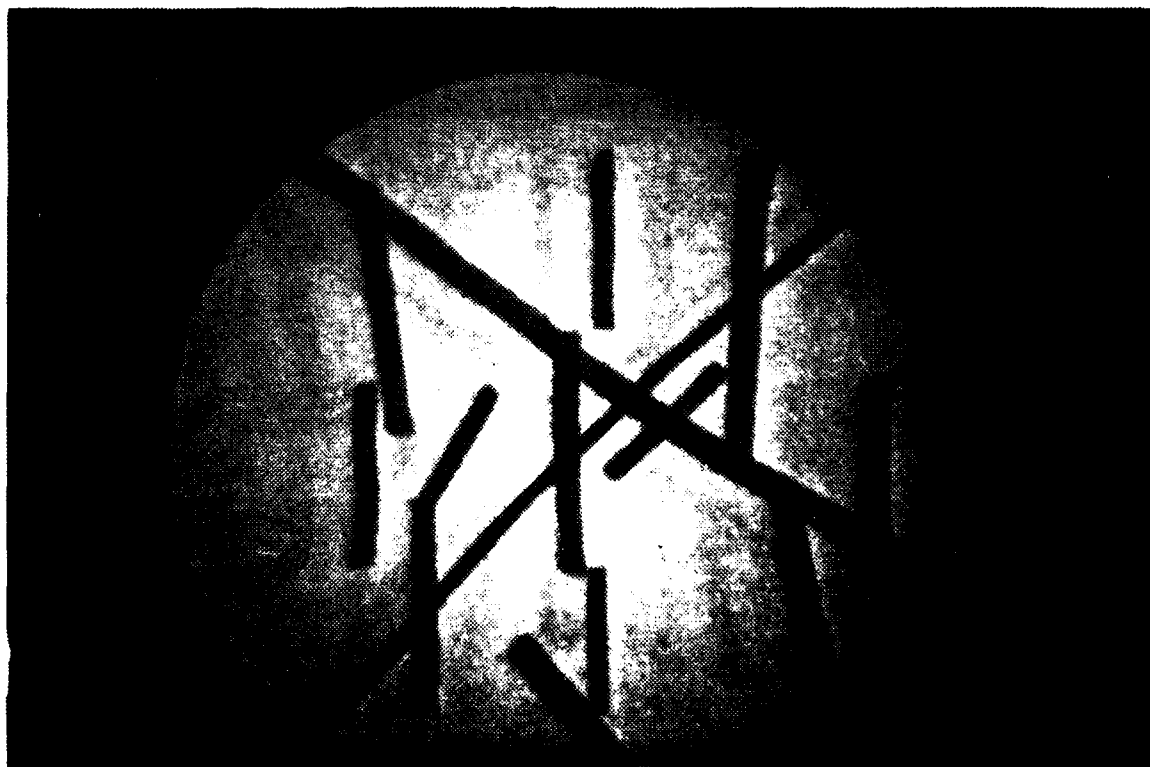
Figure 4-1c. Microfocus X-Ray Image.

appeared to be at the same depth as the object in question, an approximate value for the depth could be read out.

4.2.2   Anomaly Depth Measurement

Image processing can be used as a powerful tool in the stereo-depth determination. A code has been written and implemented on the SAIC computer-based processor that permits automated depth measurement of specified objects within a sample specimen after system calibration. The operator uses a cursor to "point" to radiographic indications and the depth, as measured from the front surface, is displayed adjacent to each indication. The technique described below is very general. It can be applied to microradiography as described above, i.e., millimeter movement of the electron beam, or to macro stereo radiography, i.e., physical movement of either (or both) the x-ray tube or the electronic imager.

When two X-ray images of the same object are obtained from different angles, depth information about features in the object can be obtained. In the following discussion, a method of obtaining this information will be presented.

A sketch of the experimental geometry is shown in Figure 4-2a. The part to be inspected is positioned between the X-ray source and the X-ray image amplifier on an x, y, z translation table so that all portions of the object can be inspected. The imager is fixed in position and, for illustrative purposes, the X-ray source is capable of shifting from position 1 to position 2. Such a shift can be accomplished mechanically by a direct translation of the X-ray tube or by the electromagnetic shift of the electron beam within the X-ray tube. The advantage of the mechanical shift approach is that any x-ray source can be used.

During the initial positioning of the part, the operator views a live X-ray image of the object as he moves the object. The operator can position the object using the x and z stages of the translation table until a feature (or features) is seen for which he wishes depth information. At this point several tnings happen. First, an integrated image is obtained with the X-ray generator at the first position. Second, the X-ray generator is moved under computer control to the second

42

X-RAY IMAGE
AMPLIFIER

PART MOVEMENT
PLATFORM

POSITION 2

X-RAY SOURCE
POSITION 1

TRANSLATION
TABLE
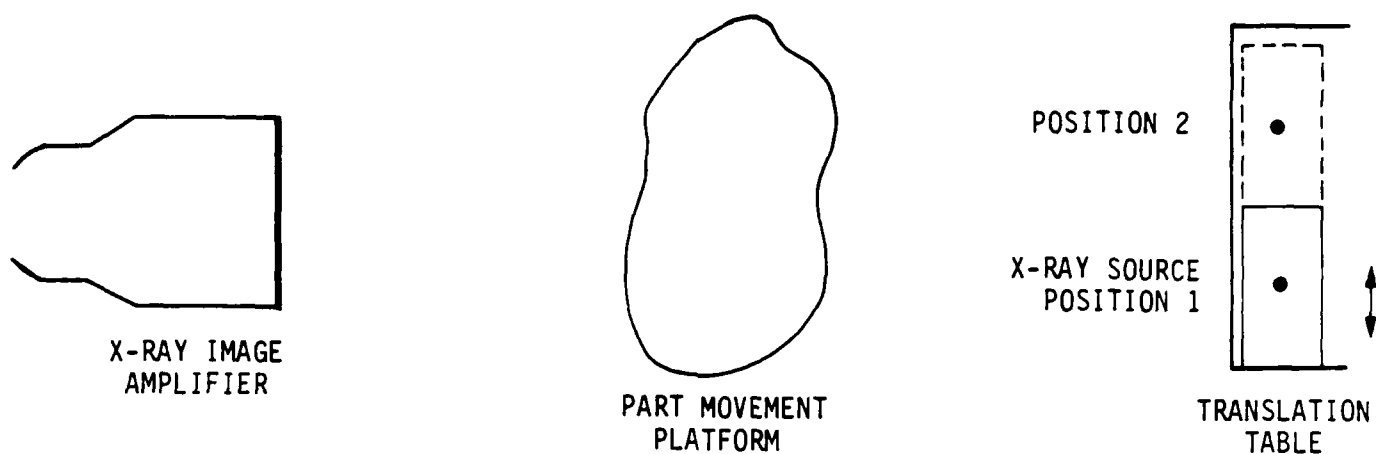
Figure 4-2a.   Sketch of Quantitative Stereo Measurement Geometries.

IMAGE 1

SOURCE
POSITION 2

POINT 1

D_1

POINT 1

POINT 2

0_S

D_2

POINT 2

POINT 1

IMAGE 2
POINT 2

SOURCE
POSITION 1

Z_1

Z_2

Z_S
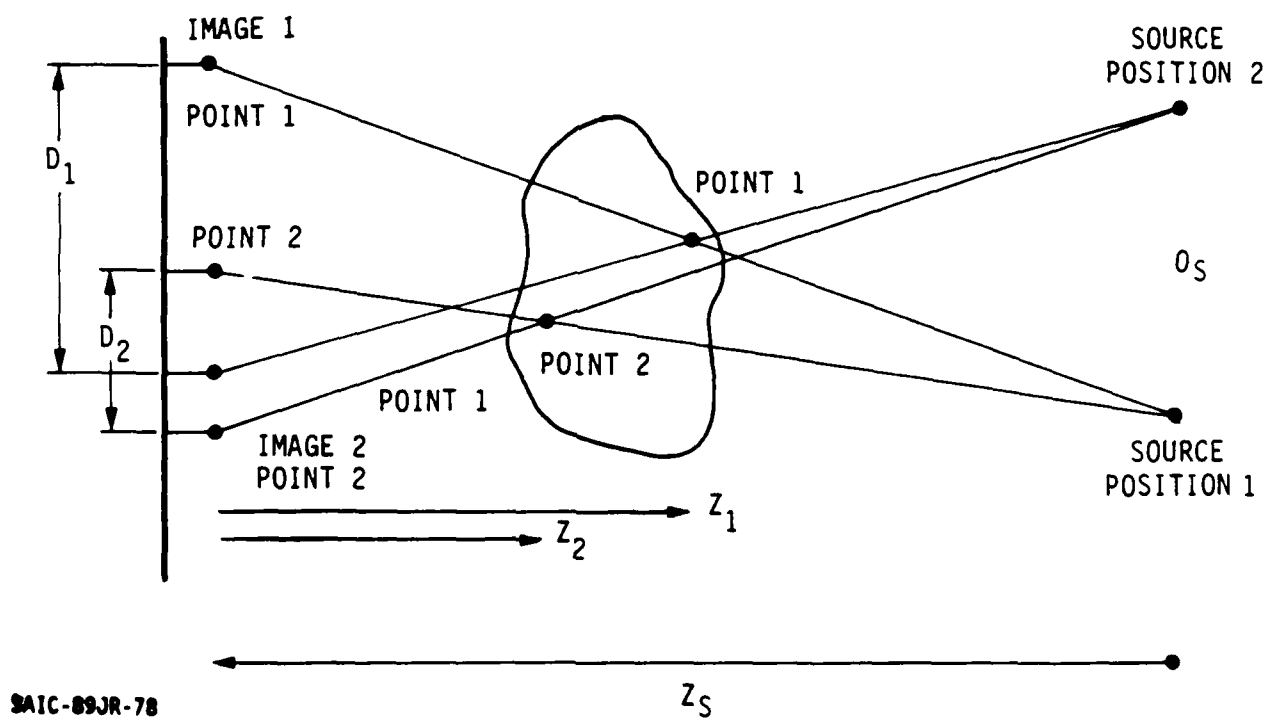
Figure 4-2b. Geometry for Quantitative Stereo Measurements.

43

position and a second integrated image is obtained. Third, the X-ray source is moved back to its original position.

At this point the operator is instructed to move a cursor to the object (he is still viewing the first image) for which he wishes depth information. The marking of several objects can be done on the same image.

When the operator indicates that he is done marking objects, the code measures the depth of each of the objects and writes this depth to the screen along side the object marked.

The measurement geometry is shown in Figure 4-2b. The positions of the X-ray images of two points are shown for the two images obtained.

The important point is that the relative displacements of the X-ray images of the points (D_1 and D_2) are related to the distances Z_1 and Z_2. This relationship is given by the equation:

$$\frac{D_i}{Z_i} = \frac{O_s}{Z_s - Z_i}$$

or

$$Z_i = \frac{D_i * Z_s}{O_s + D_i}$$

where: D_i is the displacement of the X-ray image of object i
between the two images

O_s is the linear displacement of the X-ray source
between images

Z_s is the distance between the source and the imager.

It is seen that the relationship between D_i and Z_i is not linear. Indeed, as Z_i approaches Z_s, the displacement D_i goes to infinity. One can invert the above equation, however, to produce a linear relationship. Inverting the equation

$$\frac{1}{Z_i} = \frac{O_s}{D_i * Z_s} + \frac{1}{Z_s}$$

44

and defining

$$Y_i \equiv \frac{1}{Z_i}$$

$$d_i \equiv \frac{1}{D_i}$$

It is seen that

$$Y_1 = d_i * \frac{O_s}{Z_s} + \frac{1}{Z_s}$$

which is linear.

Once the two images are obtained, a measurement of the displacement of the image of a particular object between the two views can be obtained by repeatedly analyzing the area around the designated point in the images formed by subtracting the two original images as one of these images is scrolled. When the proper scroll is used, the difference image will become flat in this area. This proper scroll is obtained by finding the minimum in the value of the variance squared in the region surrounding the designated point. The square of the variance is defined in this case as

$$\sigma_k^2 = \sum_{i,j} \frac{(D_1(i,j) - D_2(i+k,j))^2}{NUMPX} - \left[\sum_{i,j} (D_1(i,j) - D_2(i+k,j)) \right]^2 .$$

where: $D_1(i,j)$ are the data points in Image 1

$D_2(i+k,j)$ are the data points in Image 2 at a scroll in x of k pixels

NUMPX is the number of points in the histogram.

A minimum in σ_k^2 indicates the scroll at which the two original images are the most similar.

The displacement k_{min} is then used to determine the depth of the object.

Calibration consists of using the above procedure with objects of known depth. The coefficients of the linear fit are determined using a least squares technique.

This technique has been applied to several test samples, including the low-contrast ceramic sample that contained an internal crack. The results were in excellent agreement with the known condition of the sample.

4.3 SPATIAL AND CONTRAST RESOLUTION

A test object has been fabricated (of aluminum alloy) that will test not only the measurement of parallax, but also the ability of the system to detect low-contrast, small-detail flaws (see Figure 4-3). Thickness sensitivity parameters are shown in Figure 4-3a. For these flaws, image processing can play a major role in their characterization. Figure 4-3b illustrates the application of basic image enhancement (contrast stretch) on an image of this test object, all three IQI holes are visible. Contrast transforms and edge-enhancement methods are expected to produce better measurements of the flaw size and its location in the object.

Another test of image sensitivity was made using a 1/2-inch-thick aluminum plate with a standard aluminum ASTM image-quality indicator placed on the source side of the plate, i.e., the top surface (Figure 4-4).[20] This image-quality indicator had holes of 0.010, 0.020, and 0.040 inches (0.25, 0.50, and 1.0 mm) diameter. In a static mode, the two largest holes were visible on the monitor, without image processing. Note that, being on the source side, the indicator images had the greatest magnification. This, of course, is a characteristic of magnification imaging. For discontinuities deep in a relatively thick sample, there is a noticeable change in image size due to projection magnification. This can be an advantage by alerting the interpreter to the fact that the flaw is indeed near the bottom, and not the top, of the sample. In this second test, image processing was used to enhance the image to enable the viewers to detect the 1T (.010") hole (See Figure 5-4).

A third test was made with a ceramic sample. The depths of the high-contrast artifacts were measured, and the crack, a low-contrast artifact, was

46

ABSORBER
PLATES (A)

16 pl 2x2 1/16" THICK
3 pl 2x2 1/32" THICK
4 pl 2x2x.010" THICK
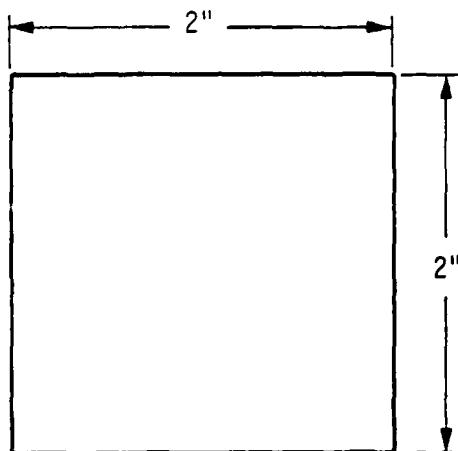
IQI
PLATES (B)

T = 1/16, 1/32, .040", .020",
.010" (ALL 2"x2")
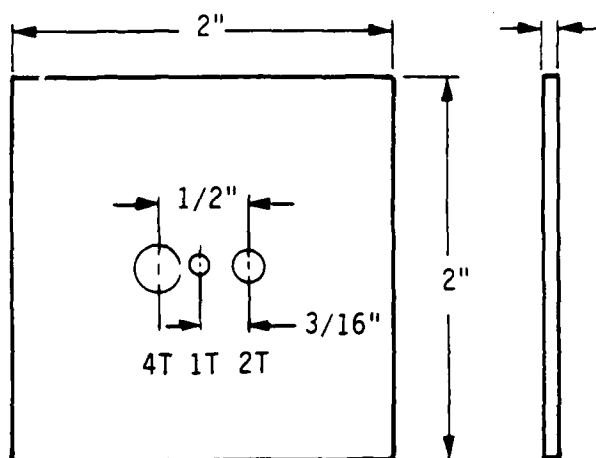
IQI PLATE TH. (T)	THICKNESS SENSITIVITY	FOR (1" SPECIMEN THICKNESS) HOLES SIZES		
		1T	2T	4T
1/16	6.2%	.062"	.125"	.250"
1/32	5.1%	.031"	.062"	.125"
.040	4.0%	.040"	.080"	.160"
.020	2.0%	.020"	.040"	.080"
.010	1.0%	.010"	.020"	.040"

*Actual Hole size = .016"

SAIC-89JR-68

Figure 4-3a. Aluminum Plates (1100 Alloy 99+% Al).
Contrast Sensitivity Test Specimen.

47
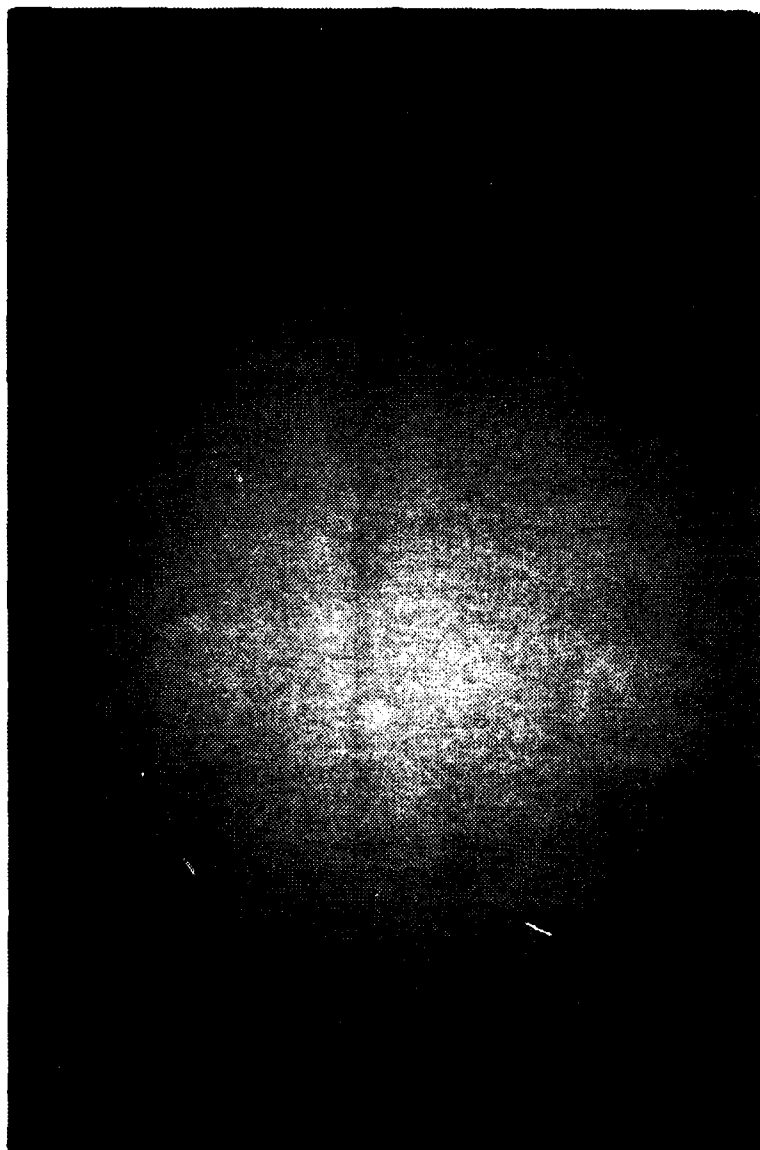
SAIC-89JR-76

Figure 4-3b. Image Processed X-Ray Image with
2% IQI. All Three Holes(4T, 2T, 1T)
are Visible.

SAIC-89JR-77
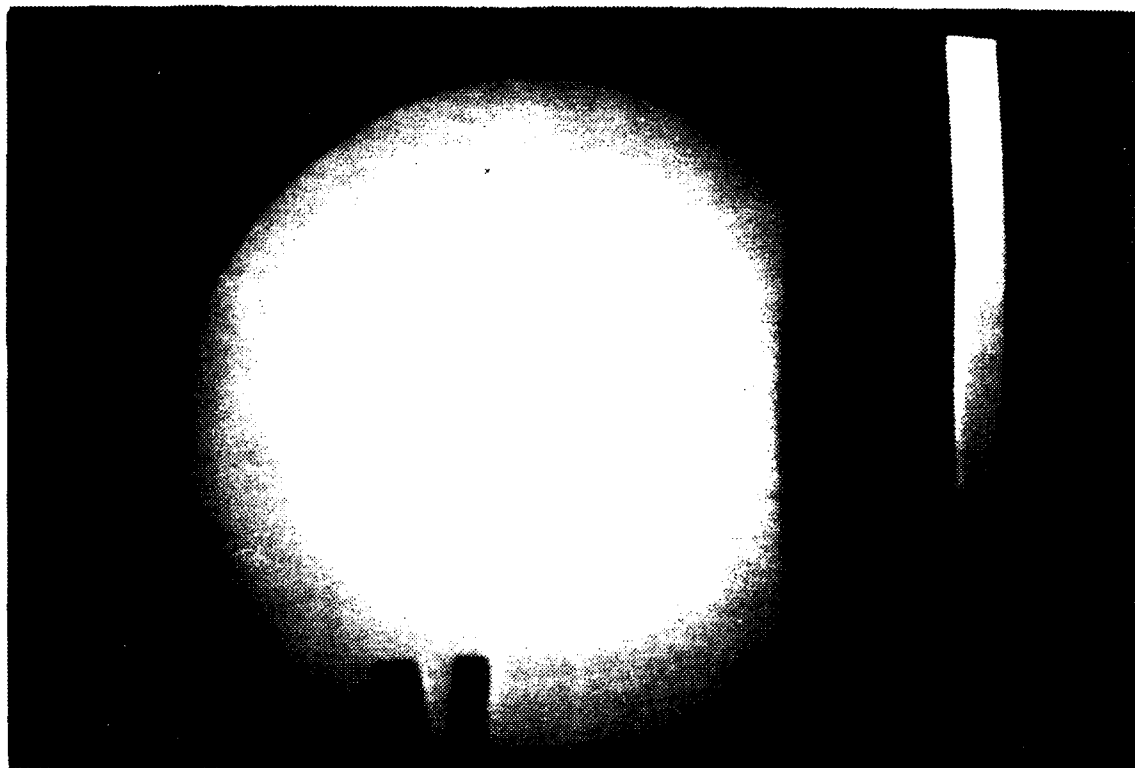
Figure 4-4. X-Ray Image of ½" Al Plate with
ASTM Penetrameter.

measurable also. There was sufficient contrast so that the crack was detectable on both left and right images. This will be required for all depth measurements, although image processing can reveal some low-contrast details that would not otherwise be revealed.

5.0 STEREO X-RAY INSPECTION APPLICATIONS

Microfocus radiology, combined with controllable switching to on-line stereo presentation, allows a very high degree of characterization of the inspected object. In many cases, almost total characterization of imbedded discontinuities is possible. For example, for small flaws and details, the location and size in three dimensions can be obtained. For relatively large flaws or details, three-dimensional locations of points within the interrogated area can be obtained and, in addition, an extensive scan of the area, using the on-line image presentation during dynamic inspections, is also possible.

In the course of development of the stereo microradiography system, a prototype was tested at Sharpe Army Depot in Lathrop, California. Many items, metals, casting, welds, ceramic, electronic components, composites, and mechanical assemblies were inspected. Some of these will be illustrated in this report, but only a live demonstration can truly show the stereo effect. For this reason, a demonstration video tape has been furnished to the Army Materials Technology Laboratory. To view it with 3-D capability will require access to the polarizing equipment used for the video display throughout this work.

The inspected samples include general-purpose items, ceramic samples and ceramic image-quality indicators, composite materials, and several electronic components. These will be discussed briefly with the understanding that most of these are on video tape. The electronics components are grouped under general-purpose items.

5.1   GENERAL-PURPOSE ITEMS

1. Figure 5-1 is an example of an IC chip which, on tape, demonstrates dramatically the stereo effect and, at the same time, because of the detail sensitivity of the microfocus source, also shows the very small connections of the IC itself to the chip terminals or lugs.

2. Figure 5-2 is an image of a dual-element vacuum tube which also lends itself well to microfocus and stereo inspection. Although vacuum tubes are not
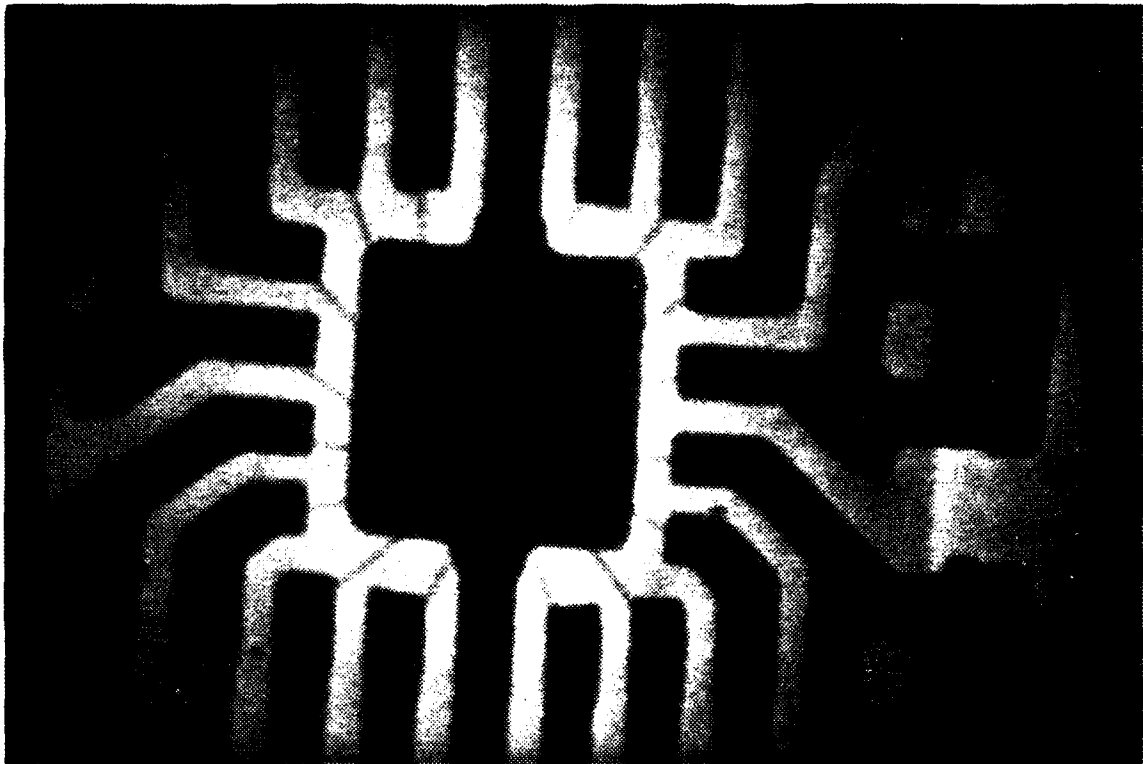
Figure 5-1. Figure IC Chip - Demonstrates High Detail Sensitivity
Due to the Geometrical Magnification made Possible by
the Microfocus X-Ray Source.
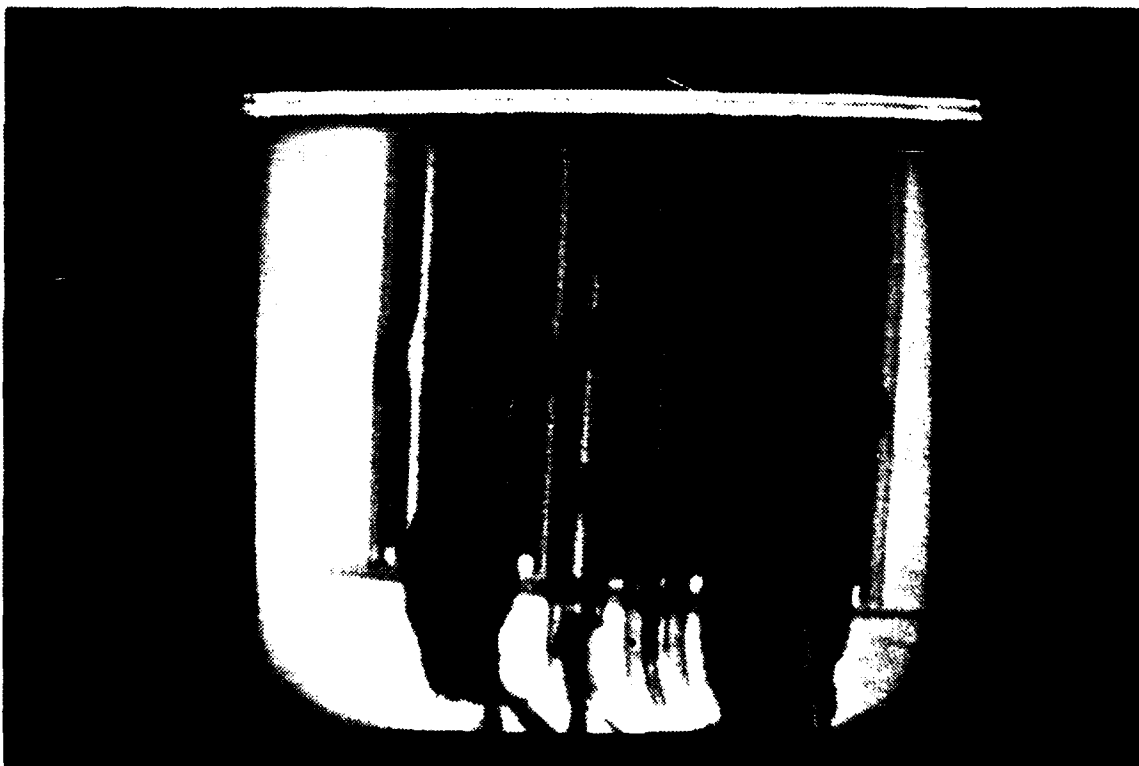
Figure 5-2. Dual Element Vacuum Tube.

likely to be an important application for stereo microradiography, similar small assemblies represent a useful application area.

3. To illustrate the good sensitivity achieved with the system in non-stereo mode, Figure 5-3 shows an image of crossed wires. This wire-image-quality indicator was furnished by J. London, Los Alamos National Laboratory. The smallest, 15μm in diameter, were readily detected in both the X and Y directions. Sensitivity was not enhanced by switching to stereo, due to the extremely small size and low contrast presented by this object.

4. A contrast sensitivity of an aluminum penetrameter (hole type) was placed on a 1/2-inch-thick aluminum plate. While contrast sensitivity was demonstrated, this object was most useful for demonstrating the value of image processing, which improved contrast and revealed all three holes in the penetrameter. Prior to enhancing, the smallest hole was not seen. This sample is illustrated in Figure 5-4.

5.2   CERAMICS

5. One of the ceramic samples inspected was a silicon-carbide sample supplied by Argonne National Laboratory, Figure 5-5. This sample shows both high-density inclusions and X-ray transparent regions (holes) in the same sample. The image demonstrates the good dynamic range available. The depth of the inclusions can be obtained by parallax measurement.

6. A high-density ceramic disk was supplied by the Naval Surface Warfare Center. This disk was approximately 1/4-inch thick, but required relatively high X-ray kilovoltage for penetration because of the high density. In spite of this, cracks within the sample were clearly revealed (Figure 5-6). Optimum crack detection was obtained by moving the disk so that the X-ray beam became aligned with the crack face.

7. Garrett-Phoenix (Allied Signal Aerospace Co.) supplied a large number of samples, mostly ceramic, for our tests. One of these was a green silicon nitride, and another a calcined silicon nitride block. Both samples were seeded
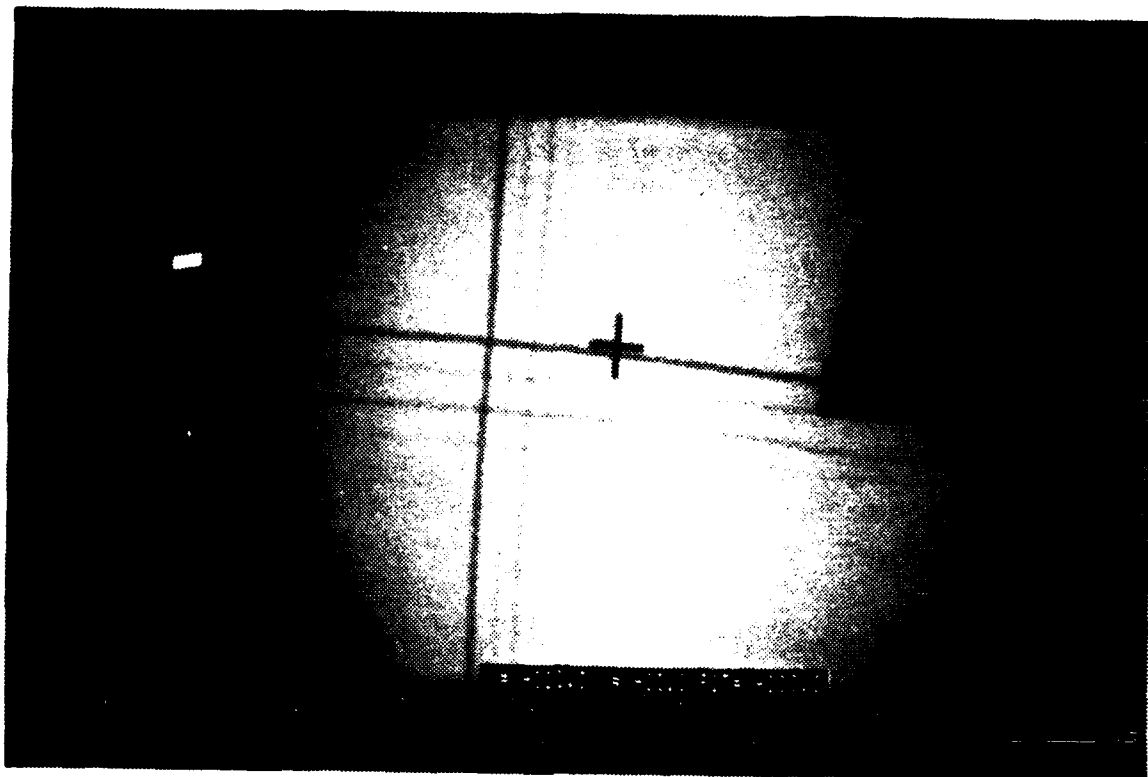
Figure 5-3. Microfocus X-Ray Result for LANL Wire Test Sample.
The Image Shows four Wires both Vertically and Horizontally.
The Smallest Diameter Wires Imaged (Slightly left of
Center) were 15 μm in Diameter.
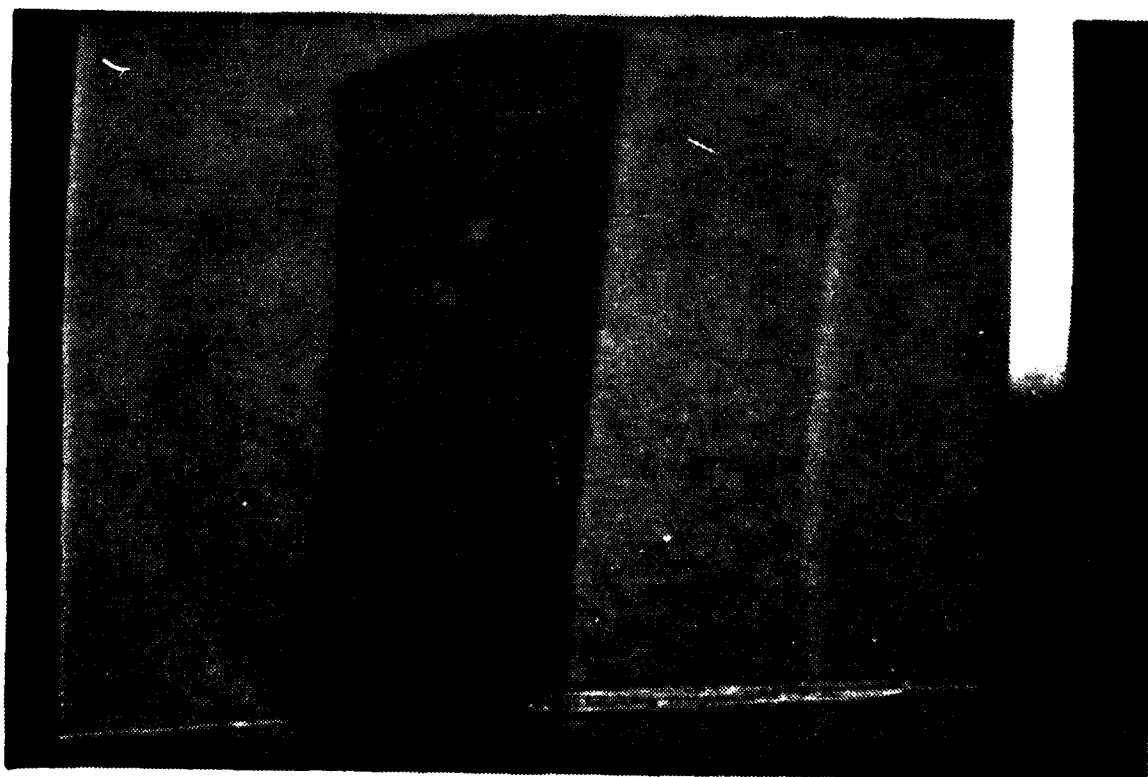
Figure 5-4. One-Half Inch Aluminum Plate with 2% ASTM
Penetrameter - Image Enhanced.

(a)
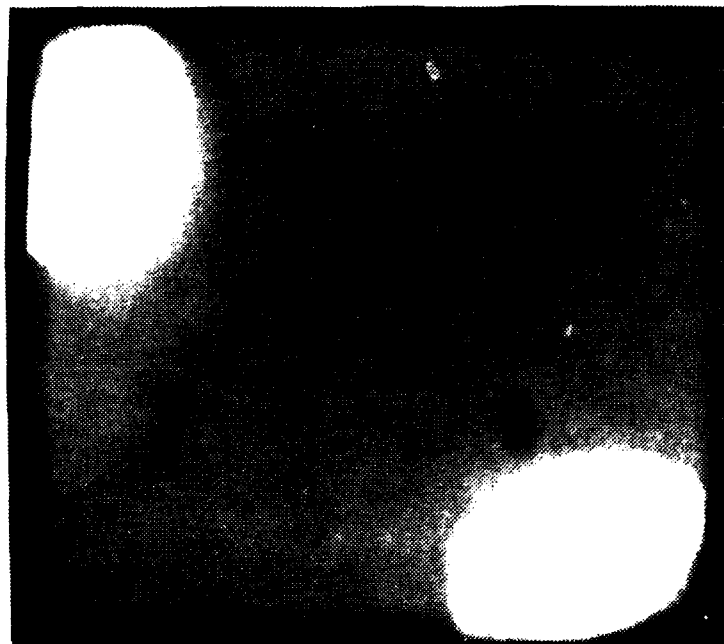
(b)

Figure 5-5a. ANL SiC Ceramic Sample (Photograph,), Microfocus X-Ray
Result 5-5b. Showing Partial Images of Axial Holes (top, left and
bottom, right) and Several High Z Inclusions.
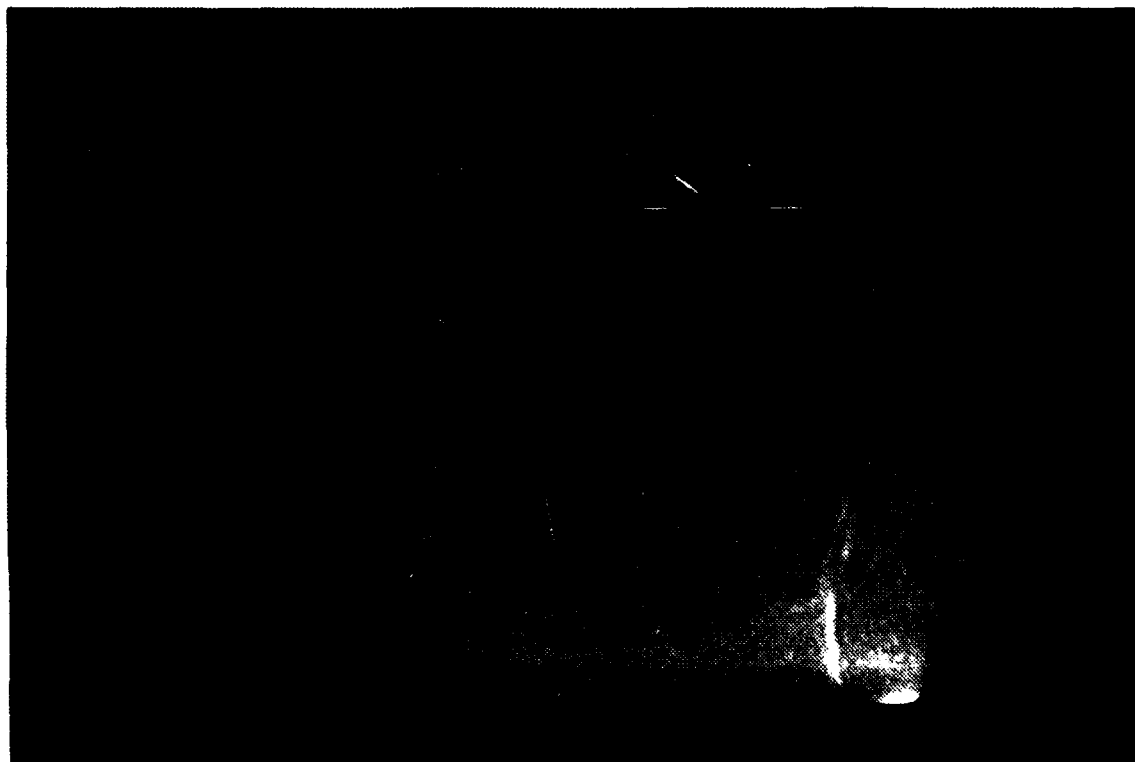
Figure 5-6. Microfocus X-Ray Result for NSWC High Z Ceramic
Sample Showing a Crack (at right).
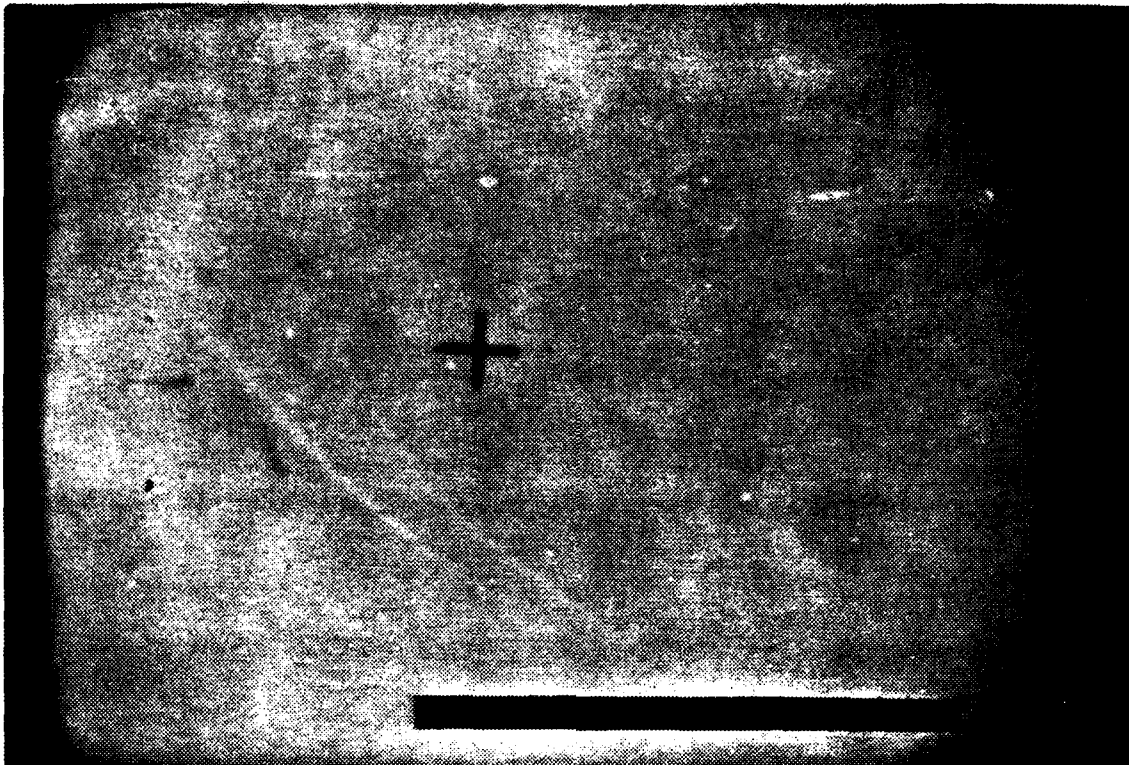
Figure 5-7a. Non-RTR Stereo-Mode Image of Silicon Nitride Ceramic with Seeded Wire Defects (dark areas), Cracks and Voids.
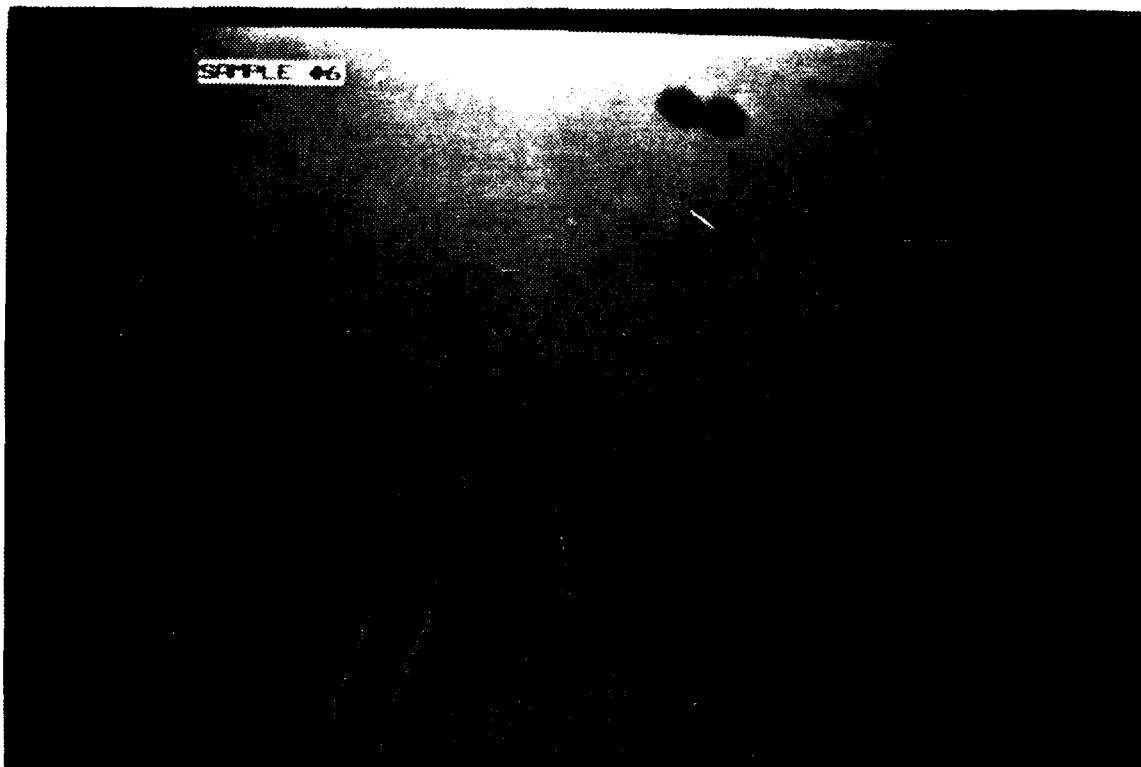
Figure 5-7b. RTR Stereo-Mode Image of Silicon Nitride Ceramic with Seeded Wire Defects (dark areas), Cracks and Voids.

with small inclusions at various places in the sample. These samples also contained cracks and voids. Some of the inclusions were as small as 50 microns. Figure 5-7 shows one of these Garrett samples in both stereo and non-stereo mode. This type of sample lends itself well to stereo presentation for identifying locations of the discontinuities.

8. Figure 5-8 represents a ceramic layered sample containing various artifacts. A similar sample was used in the Phase I work. It is a very useful sample for depth measurement, and also shows the wide variance in magnification resulting from slight changes in position of the artifacts relative to the microfocus source. While most of the artifacts are of relatively high contrast, the images also revealed a crack in one of the ceramic pieces that form the sandwich. This is shown in the illustration, and its depth in the sample, as well as the other artifacts, was easily determined by disparity measurements.

9. A ceramic with a pronounced crack is shown in Figure 5-9. This sample was furnished by the Johns Hopkins Applied Physics Laboratory. It is made from a Corning pyroceram, and is part of a radome. The dark area near the crack is part of an extra ceramic material taped to the sample to show contrast. Scanning this sample on-line revealed the total extent of the crack. In this case, the image showed that the crack curved through the thickness of the sample. It could, of course, be further interrogated by disparity measurements in stereo to reveal more detail of the curving extent of the separation.

5.3   COMPOSITES

10. Practical composite samples were furnished by John Barnes of Sharpe Army Depot. The first of these, Figure 5-10, was a composite Cobra Helicopter blade fitting. This fitting was epoxy-filled. Two oval-shaped, relatively-high-density linear inclusions are shown.

11. Another Sharpe-furnished sample was a completely boxed helicopter blade, as it would be received at the depot. Inspections were made without removing the blade (a very large object) from the box. This, of course, demonstrates the utility of the X-ray inspection technology. In addition, the
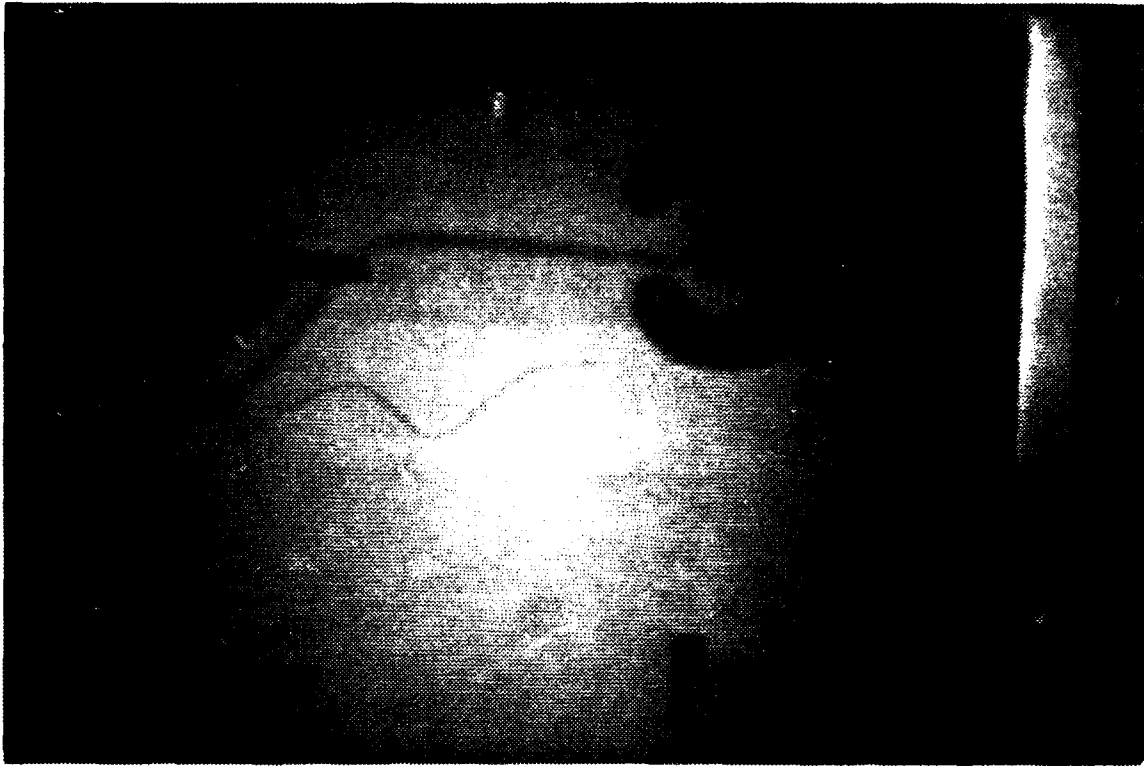
Figure 5-8. Ceramic Sandwich Supplied by
IQI, with Artifacts
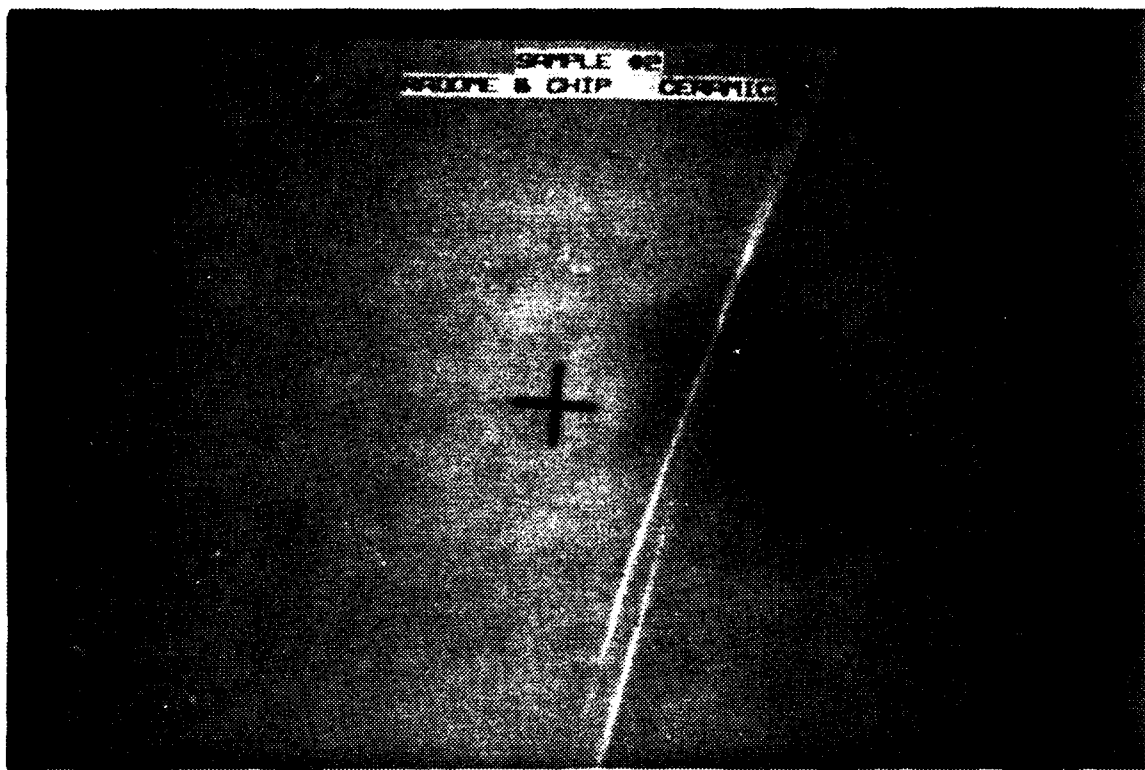
Figure 5-9. RTR Image of a Cracked Ceramic. The Double White Crack
Images show that the Crack Curved Through the Thickness.
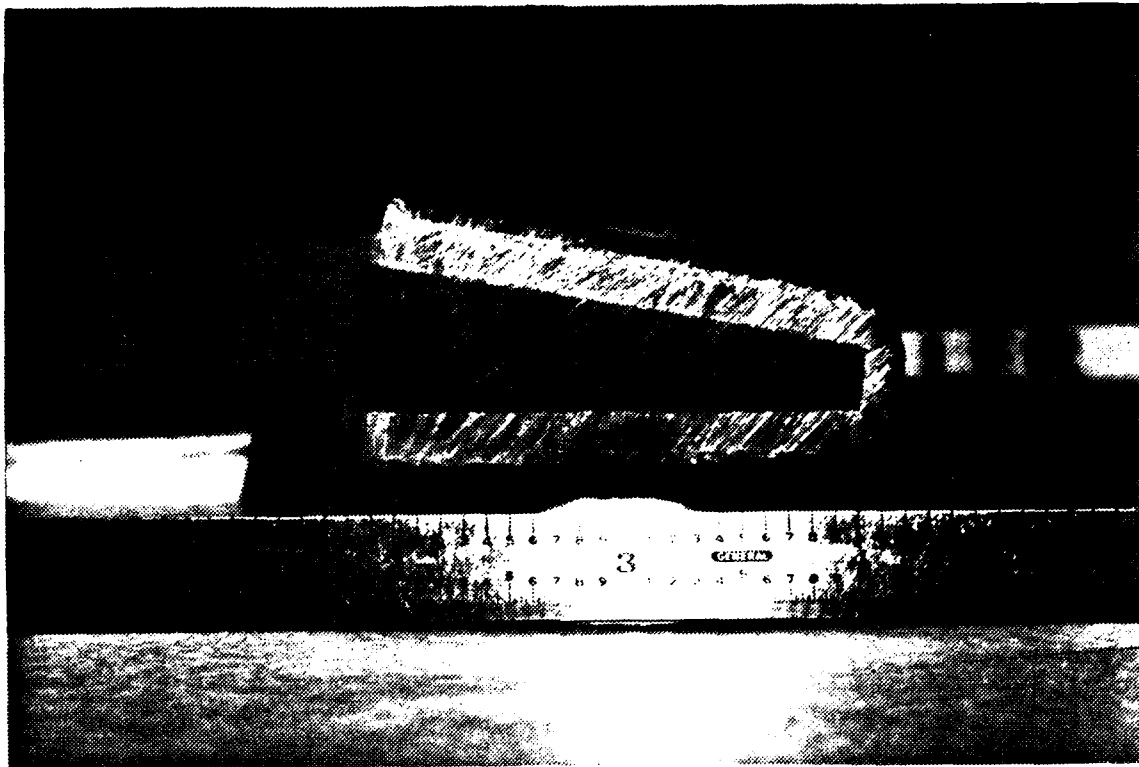
Figure 5-10a. Photograph of a Sharpe Supplied Cobra Helicopter
Composite Epoxy-Filled Rotor Blade Fitting. Image of Cavity
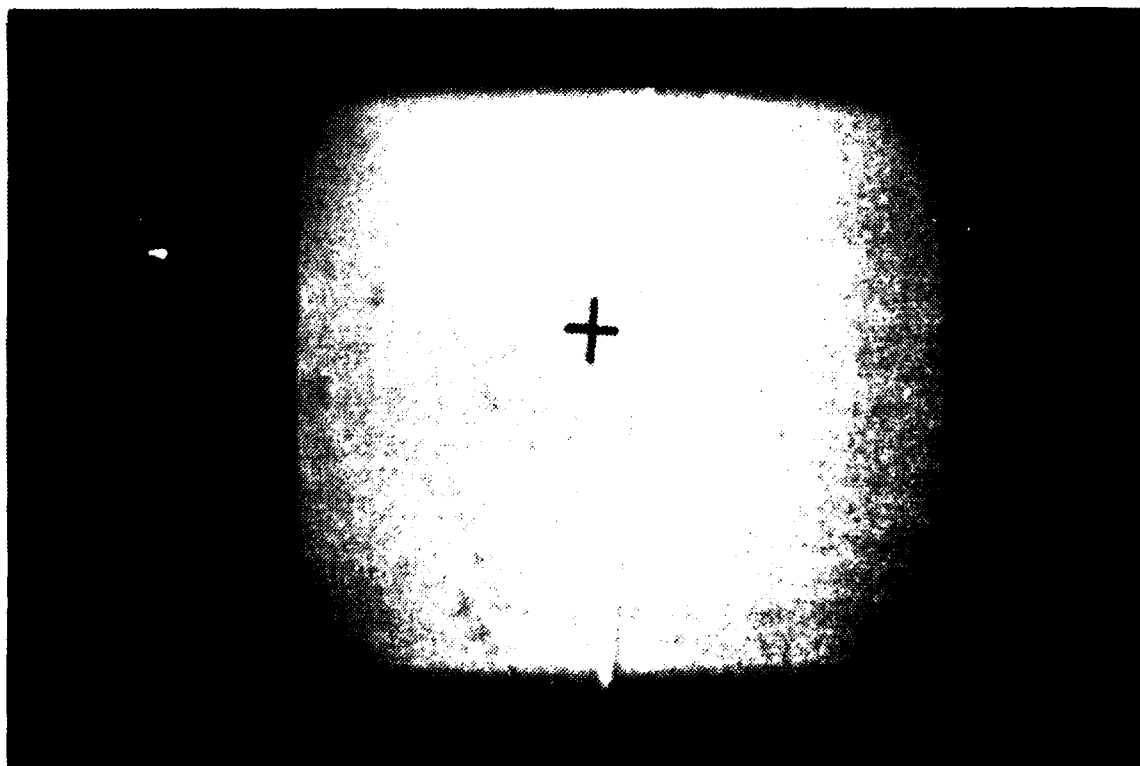in the Epoxy is Shown at the Lower Left.

Figure 5-10b. Microfocus X-Ray Result of Helicopter Fitting
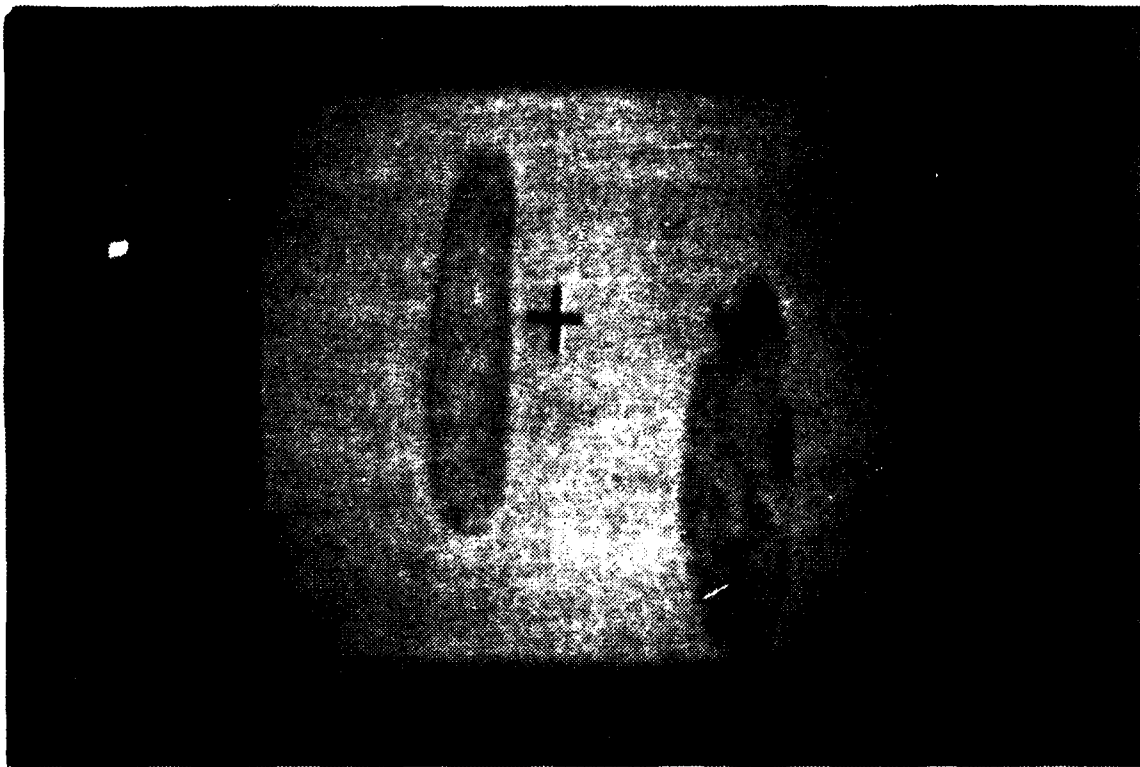Showing an Extended Linear Indication.

Figure 5-10c. Microfocus X-Ray Result of Helicopter Fitting Showing
Two Oval Shaped high Z Indication.

microfocus equipment was able to penetrate this box and blade, and reveal a large crack in the composite filling. This, of course, makes the blade unacceptable for immediate deployment to the field, and the item was subject to engineering review. Figure 5-11 shows this crack. The disparity display, in combination with on-line scanning, allowed a very good characterization of the crack, as well as the other inclusions or structure revealed by the inspection. It was easy to demonstrate that the crack and the other non-uniform structures shown were not in the same plane. In fact, some of the structures shown appear to be on the blade's surface.

12. A laminated composite furnished by Garrett was also inspected. These laminations were easily revealed by the microfocus system, and one suspicious area (possibly crack) was found during scanning. It was the opinion of both IQI and SAIC staff that this sample would benefit from use of an image intensifier capable of operating in a lower-kV range than the one at Sharpe. Figure 5-12 shows the laminations in the sample.

5.4   WELDS AND METALS

13. Two steel weld samples were furnished by the National Institute of Standards and Technology (NIST), Boulder. Figure 5-13 shows these two samples. The samples show incomplete penetration and several areas where material has obviously been removed from the sample. One image is not in stereo mode, Figure 5-13a, while the other is. Note the parallax on the stereo image of both the flaw area and the wire placed on the surface of the weld (dark area). This, of course, allows the inspector to measure the depth of the discontinuity relative to the surface.
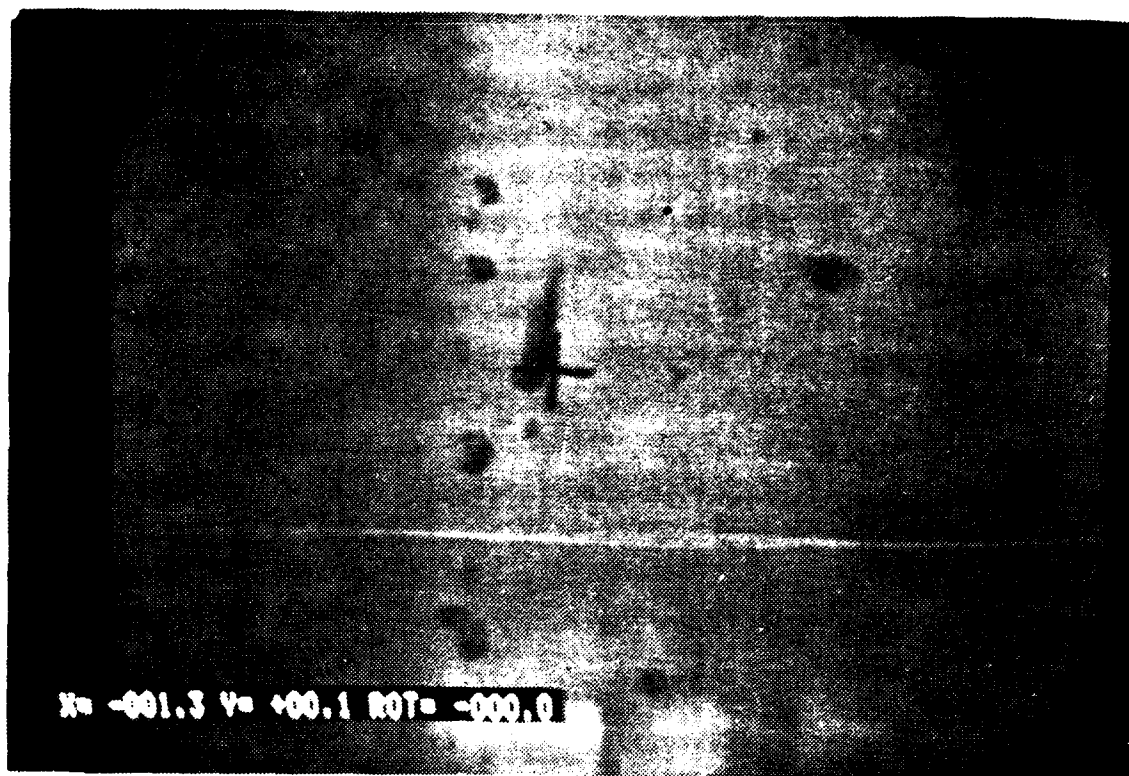
Figure 5-11a.
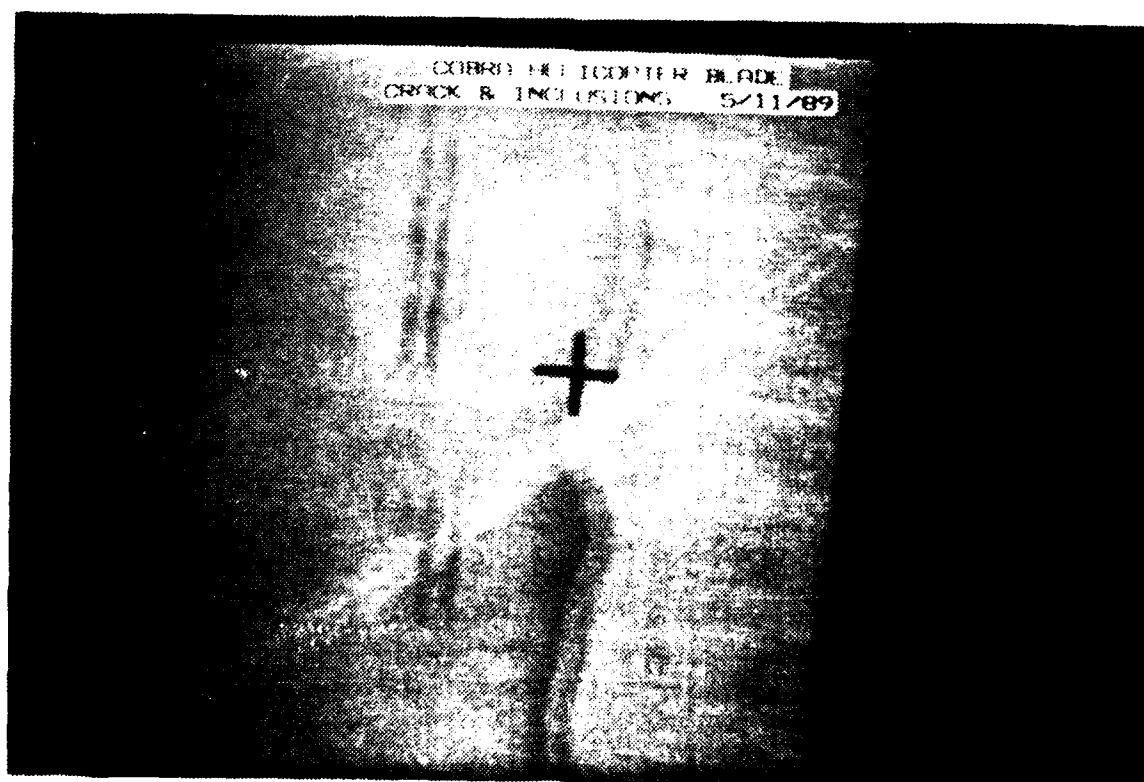
Figure 5-11b. The Crack Extended Upward in the Lower View, b. RTR
Stereo Mode Images of a Boxed Helicopter Blade Showing Several
Inclusions (dark areas), and a Long Crack (Horizontal White
Line in Upper View).
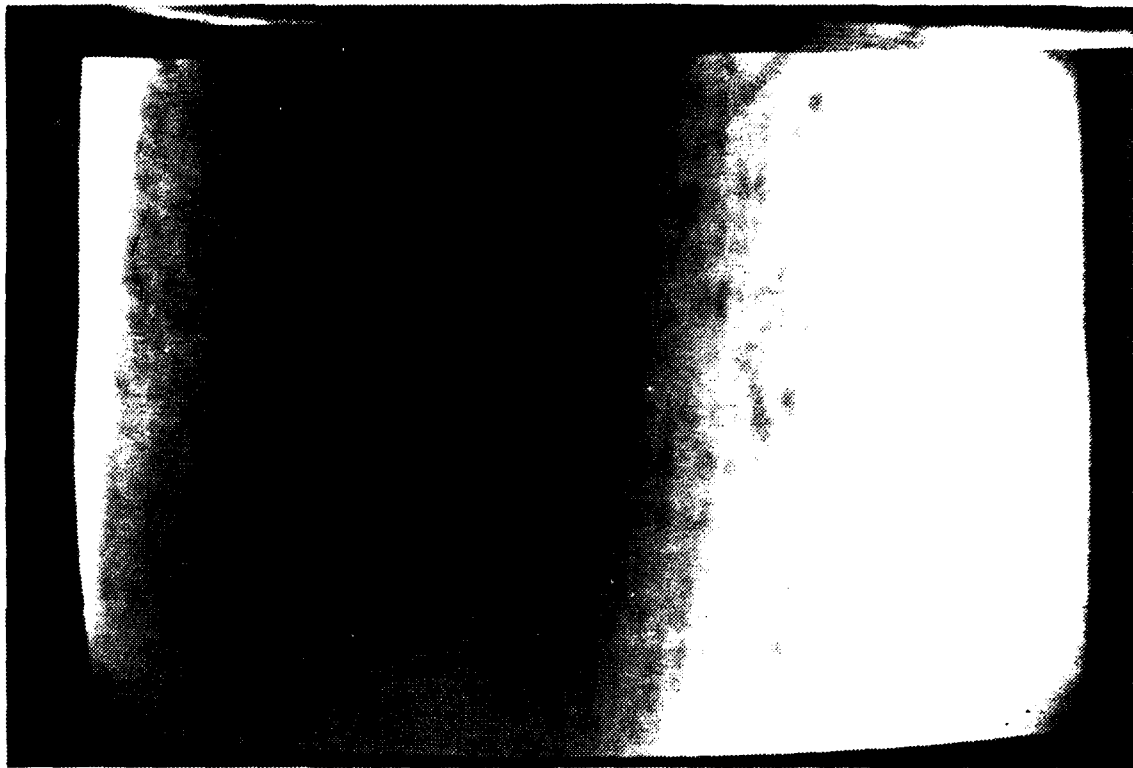
Figure 5-12a.
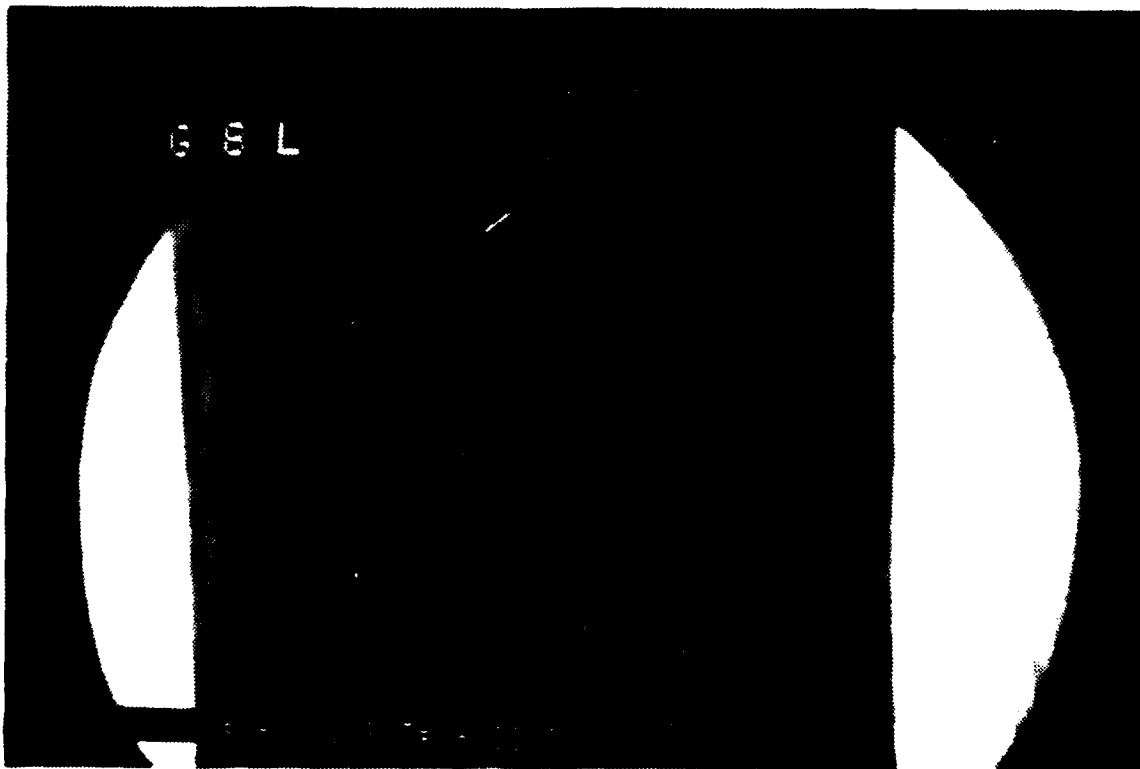
Figure 5-12b. RTR Image of a Coated Carbon-Carbon Composite. Dark
Areas are ResinPockets. Figure 5-12a is an Image Made with the
High Energy Image Amplifier. Figure 5-12b is an Image Made
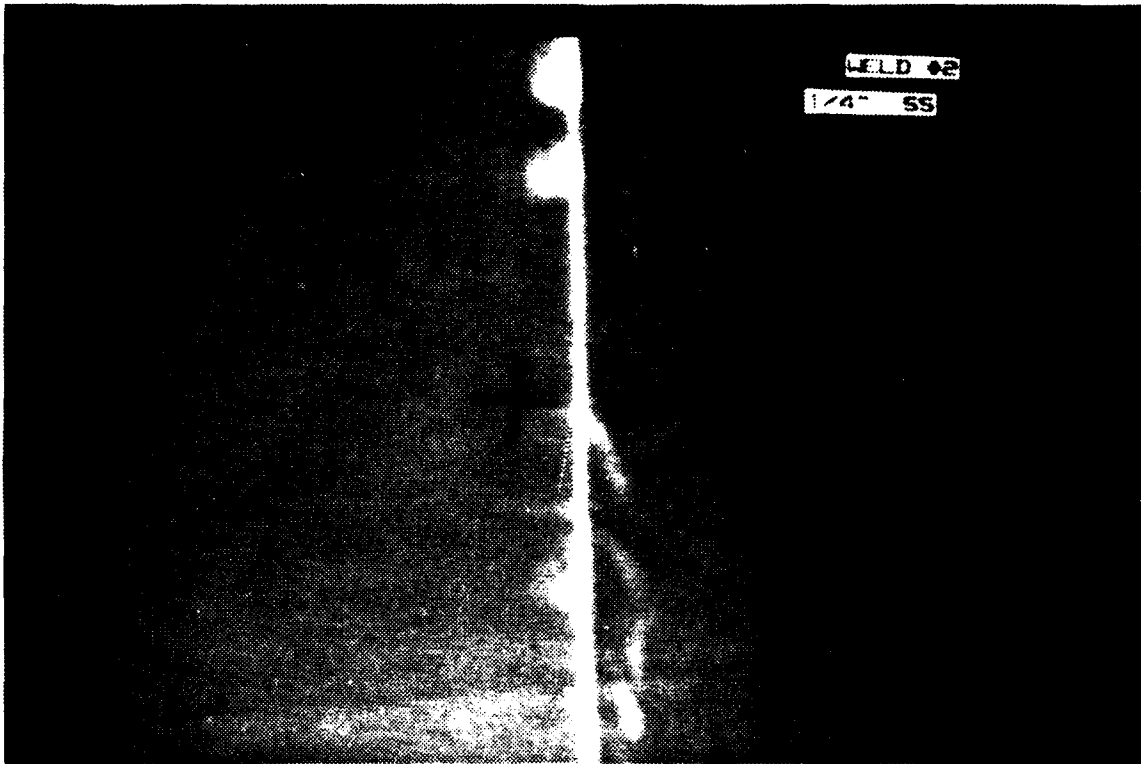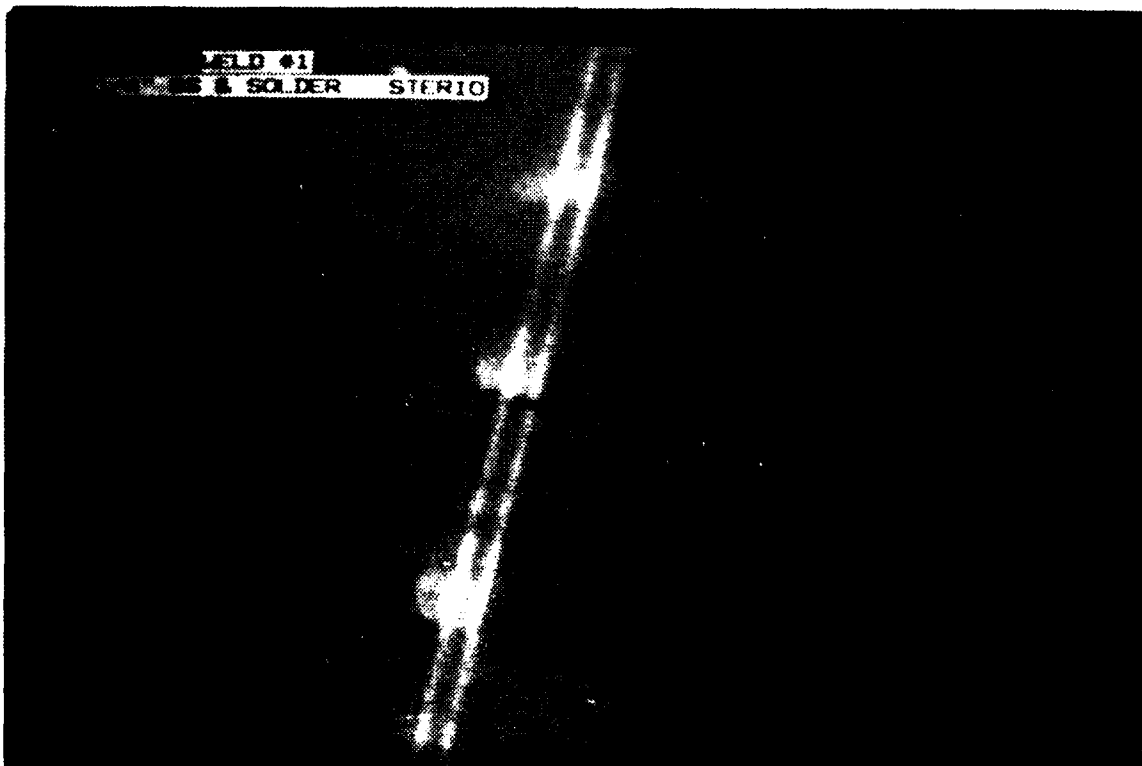with the low kV Image Amplifier.

64

Figure 5-13a.

Figure 5-13b. Real-Time Microfocus Radioscopic Views of a Steel Weld Containing Defects. Figure 5-13a is a Conventional Real-Time Image. Figure 5-13b is a Figure Showing Double Images Caused by the Stereo Mode.

6.0 PROSPECTS FOR COMMERCIALIZATION

This investigation has shown the value of the stereo-imaging method for real-time X-ray inspection. An operator can choose to view the stereo image to obtain an impression for the depth of a detail. An operator can also choose to measure the depth of one or several image details very easily and accurately. In addition, we have found that the multiple views needed for stereo viewing increase the probability of defect detection or characterization. This is particularly true for laminar defects such as cracks. These advantages make the stereo system a good prospect for commercialization.

We plan to address the stereo X-ray market in collaboration with Science Applications International Corporation (SAIC). SAIC personnel are familiar with the development by virtue of their participation in the SBIR Phase II program. In addition, the company is a manufacturer and supplier of real-time X-ray inspection equipment. Therefore, our arrangement with SAIC makes for a realistic approach to advance the stereo X-ray development to the marketplace.

By virtue of the visitors at our stereo tests at the Sharpe Army Depot and the many organizations that furnished inspection samples for those tests, we have a good list of potential customers who are already acquainted with the technique and its advantages.

The plans are to offer a complete stereo X-ray imaging system and a modification kit that can be used to adapt an existing real-time X-ray system for stereo operation. With this dual approach, the potential market for the stereo system increases greatly. Potential purchasing organizations are already being contacted to determine their level of interest.

7.0 DISCUSSION/CONCLUSIONS

The capabilities of the developed stereo microradioscopic X-ray inspection system have been well-demonstrated in this SBIR project. Stereo X-ray images can be viewed in real-time, showing object motion and displaying a three-dimensional appearance when properly viewed on a television monitor. These views provide an inspection operator with information about the approximate depth of a detail, such as an inclusion in a ceramic or component in an assembly. Several options are described to obtain an accurate measurement of depth within the inspection object. Our data show that depth measurements can be made to an accuracy of 1 mm or better. In many inspection situations, the operator may choose not to look at the stereo image, choosing instead only to measure the depths of the details of interest.

The quantitative measurement of the position (depth) of an indication relative to the article's surface or some other feature is an important capability made possible by the stereo technique. Several approaches were implemented to demonstrate quantitative depth measurements. All require the benefit of an image processor. The approaches ranged from a "3-dimensional" cursor that, when positioned on the indication, yielded the relative depth, to an automated procedure that yields <u>calibrated</u> depth information for several indications. This second approach is applicable to the full range of radiographic applications, both microradiography and standard radiography.

The microfocus X-ray inspection system provides excellent spatial resolution, with values as small as 15 μm demonstrated in this report. The contrast capability demonstrated is also attractive. Contrast well below the usual code value of 2%, or 2-2T, contrast sensitivity can be realized.

These excellent detection characteristics, coupled with stereo imaging and depth measurement, make the developed system very useful for many practical inspection problems. Application demonstrations described in this report include inspection problems related to electronics, ceramics, composites, welds, castings and electromechanical assemblies. The many inspection results achieved during the tests at the Sharpe Army Depot are highlighted by the images showing inclusions and a long crack in a completely boxed helicopter blade. The multiple views

required for stereo imaging permitted the following of the crack well beyond the range normally achieved in a conventional X-ray inspection of this large object.

Experience in working with the stereo system has led us to recognize several areas for improvement. Displaying the stereo images at 30 frames/sec produces flicker in the image which can sometimes be disturbing. There are products available which will permit changing a 60-Hz video to 120-Hz display. This faster presentation of the stereo images for display would minimize any flicker. In the matter of the ghosting effect, a gateable CCD camera would permit much of the carry-over image to be eliminated, thereby reducing the ghosting effect. These potential improvements are among those under consideration for the commercialization stage.

Plans to commercialize this new X-ray system are proceeding. Offerings will include a complete stereo X-ray system and a modification package to upgrade an existing real-time X-ray system for stereo and depth measurement capability. Modifications can be applied to either microfocus X-ray systems or to conventional X-ray imaging systems.

ACKNOWLEDGEMENTS

REFERENCES

1. St. John, A. and Isenburger, Herbert R., "Industrial Radiography," 2nd Edition, J. Wiley and Sons, New York, 1943. This book lists many early references to stereo-radiography, dating back to 1925.

2. McMaster, R.C., editor, "Nondestructive Testing Handbook," Vol. 1, Ronald Press, New York, 1959, Section 20.

3. Halmshaw, R., editor, "Physics of Industrial Radiology," Iliffe/Heywood Books, London, 1966, pp 394-401.

4. Halmshaw, R., "Industrial Radiology--Theory and Practice," Applied Science Publishers, London and New Jersey, 1982, pp 168-170.

5. Sendeckyj, G.P., "NDE (Destructive and Nondestructive Evaluation) Techniques for Composite Laminates", AGARD Conf. Proceedings 355, Characterization Analysis and Significance of Defects in Composite Materials, pp 2-1 to 2-22, London, April, 1983.

6. Rummel, W.D., Tedrow, T.L. and Brinkerhoff, H.D., "Enhanced X-Ray Stereoscopic NDE of Composite Materials", Proc. 14th Symp. NDE, pp 313-322, NTIAC, San Antonio, 1983.

7. Henneke, E.G., Russell, S.S., "Impact Damage Detection and Evaluation by Active and Passive Thermography and Stereo X-Ray Radiography in Advanced Composite Panels", Proc. 14th Symp. NDE, pp 220-237, NTIAC, San Antonio, 1983.

8. Jamison, R.D. and Reifsnider, K.L., "Advanced Fatigue Damage Development in Graphite Epoxy Laminates", Report AFWAL TR-82-3103, Wright-Patterson AFB, OH, December 1982.

9. Khalafalla, A.S., "Single Monitor Stereoradiological System Using PLZT Electro-Optical Shutters, " 29th Annual Conference on Engineering in Medicine and Biology, 438, 1976.

10. Berry, H.W. and Rice, O.F., "A Three-Dimensional Television System for Remote Viewing," Proc. 26th Conference on Remote Systems Technology, 299-305, 1978.

11. Julesz, B., "Stereoscopic Vision", Vision Research, 26, 9, p. 1601, 1986.

12. Takahashi, M., Ozawa, Y. and Takemoto, H., "Focal Spot Separation in Stereoscopic Magnification Radiography", Radiology 140: 227, July 1981.

13. Takahashi, M. and Ozawa, Y., "Stereoscopic Magnification Angiography Using a Twin Focal-Spot X-Ray Tube", Radiology 142:791, March 1982.

14. See e.g. Standard Cathode Ray Tube Phosphors, Derby Luminescents Inc./Levy West Laboratories, Enfield, Middlesex EN37QW, England. (North American Agent - United Mineral & Chemical Corp., 129 Hudson St., New York, NY 10013.

15. Jedec Publication 16-B, "Optical Characteristics of Cathode Ray Tube Screens", August 1971 (EIA).

16. Ebbeni, J., and Monfils, A., editors, "Three-Dimensional Imaging," SPIE Vol. 402, Int. Society for Optical Engineering, Bellingham, Washington, 1983.

17. Butterfield, J.F., "Survey of Three-Dimensional Television," in Optics and Photonics Applied to Three-Dimensional Imagery, SPIE Vo. 212, S. Benton and M. Grossman, editors, pp 40-47, Int. Society for Optical Engineering, Bellingham, Washington, 1979.

18. Hawkins, W.J., "Electronic Newsfront," Popular Science, April 26, 1986.

19. Fink, D.G., "Television Engineering," 22-34, Second Edition, McGraw-Hill, New York, 1952.

20. ASTM E-94-88, "Standard Guide for Radiographic Testing", Annual Book of ASTM Standards, V. 0303, p. 4, 1988.

APPENDIX
RECOMMENDED FEATURES OF A REAL-TIME STEREOSCOPIC X-RAY SYSTEM

A. <u>X-Ray Unit</u>

The kilovoltage range of the X-ray source should be in the range 15-200 kVP. The lower kV range, in general, is limited by the radiation absorption in the image-intensifier face plate. The selection of the higher kilovoltage is dependent on the product inspected. For stereoscopic systems for composite inspection, 200 kVP should be adequate for thickness ranges up to 2.5 inches.

The focal spot of the unit should be at least as small as 5 μm, with an option of varying spot size up to about 150 μm. This would allow higher target loading, with the larger focal spot increasing the unit's adaptability for item inspection.

The X-ray unit should have internal magnetic deflection coils that can be programmed from the console. The controls should maintain either a fixed focal-spot location or should be able to move from Spot 1 to Spot 2, a distance of 4-6 mm, so that alternate views (television fields) would be presented on the monitor every 1/60 of a second. This enables one to do stereo radioscopic inspections.

A beryllium X-ray window for the unit is essential to get maximum long-wavelength X-ray transmission.

B. <u>X-Ray Detector</u>

At the present state of X-ray microfocus-tube development, where fine focal spot tubes have relatively low X-ray output (low currents), an image intensifier is needed to enhance the brightness on the detector to a level where it can be picked up by a television system. (Alternatively, a separated screen system may be used with a high-resolution low-light-level video camera. This assumes that the time constant for this alternative system is low enough, though.)

72

C. Camera and Television System

A fast-response camera, such as a CCD camera, is required to pick up the image from the intensifier. This camera minimizes the "ghosting" problem that was evident when a plumbicon was used early in the program. In stereo radioscopy, where fields are presented every 1/60 of a second, the decay time of both the output phosphor of the intensifier and the camera scene decay must be minimized.

D. Mechanical-Handling System

The mechanical-handling system should be designed relative to the component inspected. The advantages of stereo radioscopy can only be fully utilized if the handling system has at least the three coordinate degrees of freedom, X, Y, and Z, plus the rotational degree of freedom around the Z axis.

E. Viewing System

A Tektronix SGS stereoscopic 3D display unit has been shown to work well for use by the observer to see the three-dimensional images when using the X-ray unit in the stereoscopic mode. A high-resolution, low-lag video monitor is required.

DISTRIBUTION LIST

No. of Copies	To
1	Office of the Under Secretary of Defense for Research and Engineering, The Pentagon, Washington, DC 20301

Commander, U.S. Army Laboratory Command, 2800 Powder Mill Road, Adelphi, MD 20783-1145
1   ATTN: AMSLC-IM-TL
1   AMSLC-CT

Commander, Defense Technical Information Center, Cameron Station, Building 5, 5010 Duke Street, Alexandria, VA 22304-6145
2   ATTN: DTIC-FDAC

1   Metals and Ceramics Information Center, Battelle Columbus Laboratories, 505 King Avenue, Columbus, OH 43201

Commander, Army Research Office, P.O. Box 12211, Research Triangle Park, NC 27709-2211
1   ATTN: Information Processing Office

Commander, U.S. Army Materiel Command, 5001 Eisenhower Avenue, Alexandria, VA 22333
1   ATTN: AMCLD

Commander, U.S. Army Materiel Systems Analysis Activity, Aberdeen Proving Ground, MD 21005
1   ATTN: AMXSY-MP, H. Cohen

Commander, U.S. Army Armament, Munitions and Chemical Command, Dover, NJ 07801
1   ATTN: Technical Library
1   AMDAR-LCA, Mr. Harry E. Pebly, Jr., PLASTEC, Director

Commander, U.S. Army Natick Research, Development and Engineering Center, Natick, MA 01760
1   ATTN: Technical Library

Commander, U.S. Army Satellite Communications Agency, Fort Monmouth, NJ 07703
1   ATTN: Technical Document Center

Commander, U.S. Army Tank-Automotive Command, Warren, MI 48397-5000
1   ATTN: AMSTA-ZSK
1   AMSTA-TSL, Technical Library

Commander, White Sands Missile Range, NM 88002
1   ATTN: STEWS-WS-VT

President, Airborne, Electronics and Special Warfare Board, Fort Bragg, NC 28307
1   ATTN: Library

Commander, U.S. Army Missile Command, Redstone Scientific Information Center, Redstone Arsenal, AL 35898-5241
1   ATTN: AMSMI-RD-CS-R/Doc
1   AMSMI-RLM

Director, U.S. Army Ballistic Research Laboratory, Aberdeen Proving Ground, MD 21005
1 ATTN: SLCBR-TSB-S (STINFO)

Commander, Dugway Proving Ground, Dugway, UT 84022
1 ATTN: Technical Library, Technical Information Division

Commander, Harry Diamond Laboratories, 2800 Powder Mill Road, Adelphi, MD 20783
1 ATTN: Technical Information Office

Director, Benet Weapons Laboratory, LCWSL, USA AMCCOM, Watervliet, NY 12189
1 ATTN: AMSMC-LCB-TL
1 AMSMC-LCB-R
1 AMSMC-LCB-RM
1 AMSMC-LCB-RP

Commander, U.S. Army Foreign Science and Technology Center, 220 7th Street, N.E., Charlottesville, VA 22901
1 ATTN: Military Tech

Commander, U.S. Army Aeromedical Research Unit, P.O. Box 577, Fort Rucker, AL 36360
1 ATTN: Technical Library

Commander, U.S. Army Aviation Systems Command, Aviation Research and Technology Activity, Aviation Applied Technology Directorate, Fort Eustis, VA 23604-5577
1 ATTN: SAVDL-E-MOS

Commander, U.S. Army Agency for Aviation Safety, Fort Rucker, AL 36362
1 ATTN: Technical Library

Commander, USACDC Air Defense Agency, Fort Bliss, TX 79916
1 ATTN: Technical Library

Commander, U.S. Army Engineer School, Fort Belvoir, VA 22060
1 ATTN: Library

Commander, U.S. Army Engineer Waterways Experiment Station, P. O. Box 631, Vicksburg, MS 39180
1 ATTN: Research Center Library

Commandant, U.S. Army Quartermaster School, Fort Lee, VA 23801
1 ATTN: Quartermaster School Library

Naval Research Laboratory, Washington, DC 20375
1 ATTN: Code 5830
2 Dr. G. R. Yoder - Code 6384

Chief of Naval Research, Arlington, VA 22217
1 ATTN: Code 471

No. of Copies	To
1	Edward J. Morrissey, AFWAL/MLTE, Wright-Patterson Air Force, Base, OH 45433

Commander, U.S. Air Force Wright Aeronautical Laboratories,
Wright-Patterson Air Force Base, OH 45433

1	ATTN: AFWAL/MLC
1	AFWAL/MLLP, M. Forney, Jr.
1	AFWAL/MLBC, Mr. Stanley Schulman

National Aeronautics and Space Administration, Marshall Space Flight Center,
Huntsville, AL 35812

| 1 | ATTN: R. J. Schwinghammer, EH01, Dir, M&P Lab |
| 1 | Mr. W. A. Wilson, EH41, Bldg. 4612 |

U.S. Department of Commerce, National Institute of Standards and Technology,
Gaithersburg, MD 20899

| 1 | ATTN: Librarian |

| 1 | Committee on Marine Structures, Marine Board, National Research Council, 2101 Constitution Ave., N.W., Washington, DC 20418 |

| 1 | Librarian, Materials Sciences Corporation, Guynedd Plaza 11, Bethlehem Pike, Spring House, PA 19477 |

| 1 | The Charles Stark Draper Laboratory, 68 Albany Street, Cambridge, MA 02139 |

Wyman-Gordon Company, Worcester, MA 01601

| 1 | ATTN: Technical Library |

Lockheed-Georgia Company, 86 South Cobb Drive, Marietta, GA 30063

| 1 | ATTN: Materials and Processes Engineering Dept. 71-11, Zone 54 |

General Dynamics, Convair Aerospace Division, P.O. Box 748, Fort Worth, TX 76101

| 1 | ATTN: Mfg. Engineering Technical Library |

Industrial Quality, Inc., 19634 Club House Road, Gaithersburg, MD 20879

| 1 | ATTN: Harold Berger |

Science Applications International Corporation, 10401 Roselle Street
San Diego, CA 92121

| 1 | ATTN: Dr. John Reed |

Allied Signal Aerospace Company, Garrett Auxiliary Power Division, P.O. Box 5217,
Phoenix, AZ 85010

| 1 | ATTN: Janet Minter, Engineering Sciences |

Argonne National Laboratory, Materials and Components Technical Division,
Argonne, IL 60439

| 1 | ATTN: Dr. William Ellingson |

EG&G Mound Laboratory, P.O. Box 32, Miamisburg, OH 45342

| 1 | ATTN: E. Dane Harvey |

No. of Copies	To

John Hopkins Applied Physics Laboratory, John Hopkins Road, Laurel, MD 20707
1 ATTN: Jim Kouroupis, Room 6-387

Lawrence Livermore National Laboratory, P.O. Box 808, Livermore, CA 94550
1 ATTN: Jerry Haskins, L-333

Los Alamos National Laboratory, P.O. Box 1663, Los Alamos, NM 87545
1 ATTN: Ron London

Sharpe Army Depot, Lathrop, CA 95331
1 ATTN: John Barnes, Bldg. 611, SDSSH-QQS

Director, U.S. Army Materials Technology Laboratory, Watertown, MA 02172-0001
2 ATTN: SLCMT-TML
1 SLCMT-IMA-V
1 SLCMT-PR
5 SLCMT-MRM-S, J. Antal (COR)

U.S. Army Materials Technology Laboratory,
Watertown, Massachusetts 02172-0001

REAL-TIME STEREO-MICRORADIOGRAPHY-
D.Polansky, R.Placious, E.Criscuolo,
E.Gaynor, and H.Berger
Industrial Quality, Inc.
19634 Club House Road
Gaithersburg, MD 20879

Technical Report MTL TR 89-96, November 1989, 84 pp-
illus-tables. Contract DAAL04-87-C-0074
Final Report

AD
(Unclassified)
Unlimited Distribution.

Key Words:

Nondestructive Testing
X-Ray
Stereo
Microfocus
Depth Measurement

A new real-time stereo X-ray imaging system is described. Fast X-ray source movement (TV field of 1/60 sec) is possible in a microfocus X-ray source by electromagnetic shifting of the electron beam. The two-view fields are combined in a TV frame for stereo viewing through a polarizing screen. Real-time, stereo X-ray images of moving inspection objects can be followed. One can view the stereo X-ray images to judge the apparent depth of an X-ray indication. One can also measure the depth of selected indications with a developed software system. This report describes the development of this novel stereo X-ray inspection system over the two-year period of this SBIR, Phase II project. Plans are being made to offer the stereo, depth measurement system commercially.